Reconstructing the infilling history within Robert Sharp crater, Mars: Insights from morphology and stratigraphy

Jeremy Brossier, Laetitia Le Deit, John Carter, Nicolas Mangold, Ernst Hauber

Reconstructing the Infilling History within Robert Sharp Crater, Mars: Insights from Morphology and Stratigraphy

J. Brossier[1*], L. Le Deit[2], J. Carter[3], N. Mangold[2], E. Hauber[4]

(1) Wesleyan University, Department of Earth and Environmental Sciences, Planetary Science Group, 265 Church St., Middletown, 06459 CT, USA.

(2) Laboratoire de Planétologie et Géodynamique Nantes, UMR 6112, CNRS, Université de Nantes, Nantes, France.

(3) Institut d'Astrophysique Spatiale, IAS, Université Paris-Sud, France.

(4) Institute of Planetary Research, German Aerospace Center DLR, Berlin, Germany.

*****Corresponding author: Jeremy Brossier (brossier.jrmy@gmail.com)

Keywords

Mars, Remote sensing, Geologic evolution, Aqueous minerals, Paleo-environments

Highlights (max. 85 characters, including spaces)

1. We produce a geologic map of Robert Sharp crater, at the dichotomy boundary.

2. Degradation of crater infillings into fretted terrain during Hesperian epoch.

3. Sedimentary or volcano-sedimentary airfall filling during Hesperian epoch.

4. Occurrence of late fluviolacustrine episodes possibly until the Amazonian period.

Abstract

Recent mineralogical studies suggest past aqueous activities in the 150-km-wide Robert Sharp impact crater, the western neighbor of Gale crater on Mars. Despite their mineralogical similarities, Robert Sharp and Gale craters display very different morphologies. Using high-resolution orbital images, we made morphological and stratigraphical analyses, as well as age determinations showing that Robert Sharp has experienced a complex geological history. This includes the formation of fretted terrain and the deposition of airfall material during the early – middle Hesperian epoch. The presence of valleys, fan deltas, and numerous aqueous minerals indicates fluviolacustrine episodes during the Hesperian epoch that persisted episodically until the Amazonian epoch between 1.3 Ga and 500 Ma. Thus, Robert Sharp and Gale craters have experienced contemporaneous aqueous phases possibly up to two billions years after the lacustrine environment recorded by the Curiosity rover within Gale crater.

1 Introduction

Robert Sharp impact crater is an open basin found along the Martian crustal dichotomy (Fig. 1, 133.59°E, 4.12°S). Open basins are described as valley-fed depressions with outlets on Mars (*Fassett and Head, 2008*). Robert Sharp has a quasi-totally degraded northern rim, no apparent ejecta blanket, and its floor exhibits mesas and knobs. Recent spectral analyses of the data collected by the Compact Reconnaissance Imaging Spectrometer for Mars (CRISM, *Murchie et al., 2007*) and the Thermal Emission Imaging System (THEMIS, *Christensen et al., 2004*) in Robert Sharp and its surroundings show that the crater and its watershed display a varied mineralogy (e.g., *Osterloo et al., 2008, 2010; Ruesch et al., 2012; Carter et al., 2015; Ehlmann and Buz, 2015*). Dark sand sheets that cover the surrounding plateaus and dark dunes within the crater floor contain olivine and high-calcium pyroxene (*Ehlmann and Buz, 2015*). Numerous chloride-rich deposits appear as light-toned materials close to clay mineral outcrops located in the southwestern watershed outside the crater (*Osterloo et al., 2008, 2010; Ruesch et al., 2012*). These chloride-rich deposits are detected using "Observatoire pour la Minéralogie, l'Eau, les Glaces et l'Activité" (OMEGA, *Bibring et al., 2005*) and THEMIS Decorrelation Stretched (DCS, *Hamilton et al., 2007*) data, and are commonly located in low-topography areas. An iron chlorine hydroxide, named akaganeite (β–FeOOH, Cl), has been detected in Robert Sharp (*Carter et al., 2015*). Akaganeite is a mineral that typically forms in acidic and saline wet

environments on Earth. Its occurrence within Robert Sharp may provide significant constraints on the ancient aqueous environment in the region (*Peretyazhko et al., 2018*). Besides the detections of akaganeite and chlorides, several deposits containing Fe/Mg phyllosilicates and other aqueous mineral phases have been observed within the crater and its surroundings (*Carter et al., 2015; Ehlmann and Buz, 2015*). Those latter deposits are usually detected at scarps in the crater rims and on fan-shaped deposits, which are located in the western half of the crater. This could indicate chemical interactions with near-neutral to alkaline waters, and hence supports the existence of past aqueous activity throughout the region. Interestingly, similar minerals have been detected in Gale crater by the Curiosity rover (Mars Science Laboratory, MSL) (*Ming et al., 2014, Vaniman et al., 2014*). Robert Sharp and Gale craters are found in adjacent watersheds.

Robert Sharp crater is either mentioned in the Martian literature for the varied mineralogy found therein (*Carter et al., 2015; Ehlmann and Buz, 2015*), the presence of fretted terrains (i.e., terrains characterized by a complicated mix of cliffs, mesas, buttes, straight-walled and sinuous canyons) at a more global scale (*Sharp, 1973*), or the fluvial processes that affected the region of both Robert Sharp and Gale craters (*Ehlmann and Buz, 2015*). Nonetheless, no detailed geological mapping of the crater has been performed. Such mapping, however, is crucial to better understand the geological history of Robert Sharp, as well as that of the watershed area. We therefore focus on constraining the hydrological and geological history of Robert Sharp crater in relation with the regional geological context. In order to reconstruct the paleo-environment in the region, we produced a geological map of Robert Sharp by combining a morphological, stratigraphical and mineralogical study of its infilling materials (section 4.1). We also performed crater counts on selected features in order to provide time constraints on the infilling history in Robert Sharp (section 4.2). Then, we discuss the possible origin of the geologic units identified within Robert Sharp (section 5) and the mineralogy detected within the crater (section 6). We propose a chronology of events to reasonably retrace its geological history (section 7). Finally, we consider the implications for aqueous activity and geochemical environments in the region of Robert Sharp and Gale craters (section 8).

[Figure 1]

2 Physiography & age

Robert Sharp crater is located between Terra Cimmeria to the south and Elysium Planitia to the north (Fig. 2a). It is very similar in size to its neighbors, Gale crater to the east (137.8°E, 5.4°S) and Knobel crater to the south (133.2°E, 6.7°S), with a diameter of ~150 km. The crater consists of an open basin towards the northern plains since its northern rim has been heavily breached (Fig. 2a). Its original eastern rim is not exposed at the surface anymore since it appears to be buried under deposits partially filling the crater and the surrounding plateau. The floor of Robert Sharp is partially filled with knobs and mesas of varied sizes and shapes forming a heterogeneous pattern. These landforms are characteristic of the so-called 'fretted terrain', as defined by *Sharp (1973)* (see section 4.1.2). Overall, the eastern part of Robert Sharp's floor raises 1.5 km higher than the western part, resulting in a west-east topographic asymmetry (Fig. 2b). The western rim rises up to 500 m of elevation, while the buried eastern rim is now at –1000 m of elevation. A THEMIS brightness temperature map (Fig. 2c) reveals low and high temperature areas in the crater. A Thermal Emission Spectrometer (TES) dust cover index (Fig. 2d) shows that only the western and southwestern parts of the crater are dust-free, corresponding to the higher-temperature areas in the THEMIS brightness temperature map from Fig. 2c (*Ruff and Christensen, 2002*). Conversely, the low temperature areas are probably covered by dust or unconsolidated sands.

[Figure 2]

Robert Sharp crater possibly formed in the Noachian epoch, based on the presence of weakly expressed valley networks incising the crater walls and the stratigraphic relationship with fretted terrains. The basement of Robert Sharp corresponds to the middle Noachian highland unit ('mNh') in *Tanaka et al. (2014a; 2014b)*. Based on stratigraphical relationships, Robert Sharp is inferred to be older than Gale (*Ehlmann and Buz, 2015*) which is expected to have been formed during the late Noachian – early Hesperian transition (*Thomson et al., 2011; Le Deit et al., 2013*). Thus, Robert Sharp possibly formed between the middle Noachian and the early Hesperian. Robert Sharp is therefore thought to have formed before or during the decline of large-scale fluvial activity in the northern highlands in late Noachian (e.g., *Fassett and Head, 2008; Irwin et al., 2005*), and before the formation of fretted terrains expected to be early Hesperian (*Irwin et al., 2004; Irwin and Watters, 2010*).

3 Data and methods

3.1 Geological mapping

We mapped Robert Sharp (Fig. 3) and defined its geological units according to their location and physical properties such as surface texture, morphology, geometry and thermal inertia. Morphologic information is provided by high resolution images of the ConteXT imager (CTX, 6 m/pixel) (*Malin et al., 2007*), providing a geomorphological context for higher spatial resolution observations acquired by the High Resolution Imaging Science Experiment (HiRISE, 25–32 cm/pixel) (*McEwen et al., 2007*). Brightness temperature variations between surface units are revealed by the Thermal Emission Imaging System (THEMIS, 100 m/pixel) in night-time infrared data (*Christensen et al., 2004; Fergason et al., 2006*). The brightness temperature of materials at the surface is directly correlated to their thermal inertia that provides information on the grain size and induration of materials within the first centimeters of the surface. High thermal inertia surfaces may indicate coarse grain-sized and/or indurated rocks exposed at the surface while low thermal inertia surfaces indicate smaller grains, poorly indurated rocks, or dust coating.

We used the global raster Digital Elevation Model (DEM) of the Mars Orbiter Laser Altimeter (MOLA), with a horizontal accuracy of about 200 m and a vertical accuracy of around 1 m (*Smith et al., 2001*) for analyzing the stratigraphic relationships between the geological units (Fig. 4). Where available, we also used the DEM from the High Resolution Stereo Camera (HRSC, *Neukum and Jaumann, 2004; Jaumann et al., 2007*) of up to 50 m grid spacing and vertical deviations from MOLA with few meters (*Gwinner et al., 2010*).

[Figure 3] – [Figure 4]

3.2 Age determination

We performed crater counts on CTX images to estimate the model ages of two fan-shaped deposits, the crater floor, and a chloride-rich deposit. The crater counts were produced using the CraterTools extension for ArcGIS software (*Kneissl et al., 2011*). Absolute model ages were determined using the Craterstats software (*Michael and Neukum, 2010*), whose models are derived from the Mars production function of *Ivanov (2001)* and the chronology function of *Hartmann and Neukum (2001)*. Only impact craters with diameters greater than 70 m were

138 considered in order to limit the effect of potential secondary craters (*Michael, 2012*) and to
139 further reduce effects of image resolution.

140 **4 Geologic map of Robert Sharp and infilling chronology**

141 ***4.1 Geologic mapping results***

142 Geological units mapped in Robert Sharp (Fig. 3) are described hereafter in stratigraphic order
143 from the oldest to the youngest. Valleys, fan-shaped deposits, and sinuous ridges are presented
144 thereafter.

145 *4.1.1 Basement and crater wall deposits*

146 The basement is the oldest unit of the region and consists of "undifferentiated impact, volcanic,
147 fluvial, and basin materials" mapped as the middle Noachian highland unit ('mNh') in the global
148 geologic map of *Tanaka et al. (2014a; 2014b)*. This Noachian unit is thought to represent parts
149 of the primitive crust of Mars formed by solidification of a primordial, molten surface and
150 bombarded by large planetesimal-size objects (*Tanaka, 1986*). Crater wall deposits are seen at
151 the foot of the southern inner rim of Robert Sharp and at the foot of an isolated basement block
152 to the north (interpreted to be a remnant of the northern rim) (Fig. 3).

153 *4.1.2 Fretted terrain*

154 The fretted terrain consists of isolated buttes with sharp-crested or flat tops, informally named
155 knobs and mesas, respectively. The term 'fretted terrain' is defined on the basis of their
156 morphology and not their lithology (*Sharp, 1973*). Their lithology can be diverse, but difficult to
157 assess from orbit. These buttes are several hundred meters to tens of kilometers-wide and are
158 several hundreds of meters to 2 km in height. The surface of the knobs and mesas is smooth and
159 flat (Figs. 5a–c). The fretted terrain is located within the crater and is extending to the north of
160 the crater towards the lowlands (Fig. 2). The fretted terrain is less abundant in the western half of
161 the crater than in the eastern half, as western mesas and knobs are relatively smaller and less
162 numerous, displaying a west-east asymmetry (Figs. 3 and 4).

163 [Figure 5]

164 *4.1.3 Draping units*

The draping deposits are observed in the eastern half of the crater and on the surrounding plateau (Fig. 3). No clear contact is seen between the fretted terrains and the draping deposits. They appear to dip parallel to the crater floor, and lie topographically and stratigraphically above the fretted terrains and the eastern nearby plateaus (Fig. 4). Draping deposits are divided into two sub-units based on their respective surface texture: Dp1 (rough) and Dp2 (smooth). The Dp1 unit shows a rough surface texture (Figs. 5d–e), and covers an area of 5200 km^2. It is commonly found in the center and eastern side of Robert Sharp (Fig. 3) where it embays and molds knobs and mesas (Fig. 5f). The Dp2 unit appears to be stratigraphically above the Dp1 unit (Figs. 5d–f) and it has a smoother surface texture than the Dp1 unit (Fig. 5e). With an area of about 5000 km^2, the Dp2 unit extends to the plateau to the east of Robert Sharp where it appears to mantle Gale's ejecta.

4.1.4 Polygonal ridges

Polygonal ridges are locally crosscutting the draping deposits and a few mesas of the fretted terrain (Fig. 3). They form networks of light-toned ridges exposed as isolated patches, randomly distributed across the draping units and the fretted terrains. They range between –1100 m and –2130 m in elevation (Fig. 5g). Ridges are heterogeneous in size and shape, each ridge varying from one hundred of meters to several hundreds of meters in length, and several tens of meters in width (Fig. 5h). Ridges do not intersect with preferential angles within the ridge networks.

4.1.5 Crater floor deposits

The crater floor deposits are found at the bottom of Robert Sharp (Fig. 3). The crater floor deposits mostly occupy the southern and northern sections of the western half of Robert Sharp (Fig. 6a). They cover-an area of about 6660 km^2 and are exposed in the lower part of the crater, down to –2700 m altitude (Fig. 4). This unit embays knobs of the fretted terrain and is thus stratigraphically above and younger than the fretted terrain. Traces of akaganeite have been detected in local depressions jointly with clays and possible carbonates (*Carter et al., 2015*). The diverse mineralogy within the crater is better described in section 6.

[Figure 6]

4.1.6 Valleys, fan-shaped deposits and sinuous ridges

Valleys have been deeply incised into the southwestern and western walls of Robert Sharp (Figs. 6b–c). Most of them are several tens of kilometers long, rectilinear to slightly sinuous in planview, and with poor tributary development. Only the southernmost valley (Fig. 6c) has multiple tributaries and is several hundred kilometers long, with a valley head within the highlands north of Herschel crater (*Irwin and Howard, 2002*). Additionally, this valley appears to be interconnected by several shallow basins along its network, identified as 'intravalley basins' in *Irwin and Howard (2002)*. Valleys breaching Robert Sharp walls are approximately 1–2 km wide, and the depth is around 250 m in the western valleys and around 1 km in the southernmost valley. They have little to no tributary development along their entrenched lower reaches inside the crater rim.

Well-preserved fan-shaped deposits are located at the terminus of some valleys, at the northwest (132°43'E, 3°37'S) and southwest (132°53'E, 5°7'S) of the crater (Figs. 7a–b). The northwestern fan-shaped deposit (84 km^2) and the southwestern one (142 km^2) superpose the crater floor deposits. The two deposits present flat-topped surfaces with some evidence of channelization. Their distal margin is clearly outlined by frontal scarps at about –2400 m in elevation (Figs. 7c–d). Given the lack of remnant buttes close to the fan-shaped deposits, the present frontal scarps may be close to the primary depositional front with limited backward erosion. The longitudinal profiles of the fan-shaped deposits show gently sloping tops with an average plain gradient of about 1–2 degrees (3% slope) over a length of approximately 10 km, followed by steeply dipping fronts that abruptly merge into the adjacent plains. The frontal scarps have been estimated to dip 6–11 degrees (10–20% slope) on the basis of HRSC DEM data. Both deposits reach thicknesses between 100 and 300 m. This thickness is certainly not uniform over the entire fan-shaped deposits surface and decreases towards the apex, as the fan-shaped deposits are superposed on sloping crater walls. Their surfaces are partially covered by dark materials probably derived from the dune fields present on the southern section of the crater floor deposits. Phyllosilicates have been detected located within scarps in the fan-shaped deposits (*Ehlmann and Buz, 2015*). Their spectral signature is identical or near identical to those found in the southern plateau alongside the chloride deposits (*Osterloo et al., 2008, 2010; Ruesch et al., 2012*). More details about the phyllosilicates and chlorides deposits are provided in a later section (section 6).

[Figure 7]

Several sinuous ridges are observed on the crater floor deposits (Fig. 6d). They are poorly ramified and are oriented parallel to the direction of the steepest slope. The length of these ridges does not exceed 10 km long. Their width is usually of several tens of meters and varies along the ridges. The spatial resolution of MOLA and HRSC DEM topographic data do not permit to measure the height of these ridges. Measurements of the length of ridge shadows provide an approximate height of several meters.

4.2 Age of selected geologic units in Robert Sharp crater

Crater counts were performed on the fan-shaped deposits, the crater floor deposits as well as the chloride-rich deposits located on the plateau south of Robert Sharp. No crater counts have been done on the fretted terrain, which appears to be covered with a dusty mantle (Fig. 2c) preventing any reliable crater counts. The estimated ages of the southwestern and northwestern fan-shaped deposits are about 1.43 ± 0.58 Ga and 512 ± 83 Ma, respectively (Figs. 8a–b). Crater counting in the southwestern fan-shaped deposit points to a resurfacing event at ~120 Ma. This suggests a recent episode of sediment deposition and erosion with at least one episode of fluvial reworking, or aeolian degradation. These results are consistent with those obtained by *Ehlmann and Buz (2015)*, and correspond to early – middle Amazonian ages.

The two fan-shaped deposits are stratigraphically above the crater floor deposits that have an estimated age of ~3 Ga, which corresponds to the late Hesperian – early Amazonian boundary (Fig. 8c). *Ehlmann and Buz (2015)* estimated an older age of ~3.6 Ga for the floor of Robert Sharp considering the floor of the whole crater (including the fretted terrain and draping deposits) without distinguishing the different infilling units in the crater.

We also performed the crater counts on a local depression exhibiting chloride-rich deposits initially detected in *Osterloo et al. (2008, 2010)* and *Ruesch et al. (2012)*. Those deposits are located on the neighboring plateaus at the southwest of the valley entrance to Robert Sharp and west of Knobel (131.94°E, 6.4°S, bottom-left corner in Fig. 3). Fig. 8d reveals that this depression has an Amazonian age, about 1.12 ± 0.33 Ga, similar within uncertainties to that of the southwestern fan-shaped deposit. *Ehlmann and Buz (2015)* also estimated a similar age of 1.1 ± 0.3 Ga. These results suggest a synchronous formation of these chloride-rich deposits and the southwestern fan-shaped deposit.

[Figure 8]

The two fan-shaped deposits and the chloride-basin are very small areas (84–142 km^2 and 36 km^2, respectively) that may not yield reliable, representative ages because they may not include any less numerous, typically more widely-spaced larger craters that would be captured in statistics covering a larger area (e.g., *von der Bogert et al., 2015; Warner et al., 2015; Palucis et al., 2020*). As a result, the statistics obtained may reflect an artificially young age for these surface units. Although the crater counts are subject to associated statistical limitations, we observe that the relative age of these small areas is consistent with stratigraphic relationships, when existing. By putting together their superposition relationships and crater counts, the fan-shaped deposits and chloride-basin are younger than underlying units, further constraining their formation to Hesperian or after (see also *Ehlmann and Buz, 2015*).

5 Interpretation of the geological units

5.1 Fretted terrain

The fretted terrain present in Robert Sharp is similar in shape and size to that commonly found elsewhere along the crustal dichotomy, between the southern highlands and the northern lowlands. It consists of plateaus, mesas, knobs and mounds in a highly irregular configuration separated by wide, flat-floored channels, valleys and troughs (*Sharp, 1973; Carr, 1995*). These landforms are commonly interpreted to result from the erosion of a thick pile of material with weak properties that could have accumulated from sedimentary or volcano-sedimentary processes (*Tanaka, 1986; Maxwell and McGill, 1988; Fassett and Head, 2007*). To date, the origin and development of the fretted terrain on Mars remains poorly understood. No mineralogical analysis has been performed yet on mesas and knobs within Robert Sharp, probably due to the lack of CRISM data at high resolution and the abundance of dust in the region (Fig. 2d). Due to the location of Robert Sharp, the mesas and knobs found there could be part of a vast fretted terrain in Aeolis Mensae (10°N–10°S, 120°–150°E). Interestingly, morphologic and thermal observations by *Irwin et al. (2004)* suggest that the fretted terrain in Aeolis Mensae is composed of friable sedimentary materials. These materials differ compositionally from the older highland materials but may resemble the sediments from the younger Medusae Fossae terrains. Medusae Fossae layered materials are thought to be made of

281 friable and variably consolidated deposits, such as dust, volcanic ash (*Scott and Tanaka, 1982;*
282 *Bradley et al., 2002; Mandt et al., 2008; Kerber et al., 2011*), or even ice-rich polar deposits
283 (*Schultz and Lutz, 1988; Head and Kreslavsky, 2004*). All these proposed origins imply
284 atmospheric transport and airfall deposition of sedimentary materials that could be responsible
285 for deposits forming the fretted terrain.

286 Many different hypotheses were proposed to explain the apparent break up and removal of such
287 material: (1) fluvial and aeolian erosion (*Breed et al., 1982; Carr, 1995; McGill, 2000; Irwin et*
288 *al., 2004*), (2) subsurface removal by groundwater flow (*Carr, 1995; Carr, 1996*), and (3)
289 faulting and tectonism (*Sharp, 1973; Irwin and Watters, 2010*). *Breed et al. (1982)* posit that
290 fretted terrains may result of an important aeolian deflation and mass wasting overprint on a
291 landscape initially carved by running water. More recent analyses (e.g., *Denton and Head, 2018*)
292 tend to favor fluvial and groundwater activity as possible fretting processes. Nonetheless, further
293 examinations at larger scale are required to assess the relative proportions of surficial and
294 subsurface hydrous activity (overland flow, groundwater flow, and ice melting) as mechanisms
295 for removal of material from the fretted terrains. Nowadays, little to no evidence of former
296 fluvial activity coeval to the fretted terrain degradation remains in Robert Sharp floor. Therefore,
297 most flow paths or other evidence must have been completely masked by later significant, non-
298 fluvial degradation.

299 It has been suggested that the materials forming the fretted terrain were deposited during the
300 early Hesperian epoch, at around 3.7–3.6 Ga (*Irwin et al., 2004; Irwin and Watters, 2010*), hence
301 shortly after the impact that formed Robert Sharp basin. *Fassett and Head (2007)* estimated the
302 formation and erosion time of the fretted terrain to range between 100 and 300 Ma, involving an
303 erosion relatively shortly after their formation during Hesperian. Moreover, the lack of an
304 observable central peak in Robert Sharp (unlike its neighbors: Gale and Knobel craters) could be
305 related to its older age, implying more erosion of its peak and rims, followed with more
306 deposition of the materials that were degraded into fretted terrains.

307 ### *5.2 Draping deposits*

308 The draping deposits (Dp1 and Dp2 units) are mostly found in the eastern half of Robert Sharp
309 and on the eastern surrounding plateaus towards Gale. No volcanic candidate landforms such as

lavas flows with lobes or vents are observed, suggesting that the draping deposits did not form as volcanic flows. Considering their location both in a depression and on plateaus, a lacustrine origin seems dubious. The high elevation of the eastern plateau-would imply an extremely deep lake (~2 km deep). We found no confining topography on the eastern plateau that would enable ponding to form a lake between Robert Sharp and Gale craters. Likewise, no fluvial channel, sinuous ridge, or apparent cross-bedding have been observed within the draping deposits, implying that a fluvial origin is also unlikely. The draping deposits mantle and are conformable to the basement. We therefore favor that these deposits may correspond to airfall and/or aeolian material consisting of fine-grained erodible sediment, such as dust, volcanic ash, and aeolian sand (like the fretted terrain).

Deposits having similar erosional aspect with relatively weak material are observed in the Medusae Fossae Formation (MFF) and may have the same origin as our draping deposits. *Ojha and Lewis (2018)* recently suggested that such deposits could be consistent with extremely porous (low-density) material like volcanic ash deposits. The presence of such airfall material has been predicted in Gale crater from orbital analyses, and are expected to be a major component of the 5 km-high Gale central mound, Aeolis Mons (e.g., *Le Deit et al., 2013*). Thus, Robert Sharp draping deposits may share common origin with some deposits of Aeolis Mons. Most sedimentary rocks in Gale are thought to have been deposited, buried, lithified, exhumed, and eroded before 3.3–3.1 Ga (*Grotzinger et al., 2015*). Considering that the crater floor deposits that presumably postdate the draping deposits are inferred to be ~3 Ga in age (Fig. 8c), the draping deposits in Robert Sharp may be older than 3 Ga and therefore deposited coevally with some deposits of Aeolis Mons in Gale crater.

5.3 Valleys, sinuous ridges, fan-shaped deposits, and crater floor deposits

Valleys incised along Robert Sharp's western walls are short and rectilinear, and have only few tributaries and display theater-like valley heads. These characteristics are often considered to be associated with valleys formed by groundwater seepage rather than surface runoff (e.g., *Sharp and Malin, 1975; Harrison and Grimm, 2005; Pelletier and Baker, 2011; Baker et al., 2015*). Such valleys often terminate in small and pristine scarp-fronted deposits, which exhibit little or no fan-head trenching or incision of the outer bounding scarp (e.g., *Irwin et al., 2005; Hauber et al., 2013*). *Lapotre and Lamb (2018)* argue that seepage erosion can only occur in loose or

weakly consolidated rock and not in competent rock like the Noachian basaltic bedrock. According to experimental observations (*Howard and McLane, 1988; Marra et al., 2014*), valley formation by seepage is limited to narrow ranges in aquifer permeabilities and sediment sizes that are characteristic of loose sediment. Nonetheless, a combination of groundwater and surface flows can explain the valley erosion in the basaltic basement (e.g., *Lamb et al., 2006; Pelletier and Baker, 2011; Amidon and Clark, 2015*). As for the southernmost valley, it is longer and more sinuous. This appears to be a typical example of a well-developed valley network incised by runoff on Mars (*Carr, 1996; Irwin and Howard, 2002*). Its lower reaches could have been reactivated coevally with the western valleys. The crosscutting of the western valleys into fretted terrain suggests a brief reactivation of highland fluvial activity after the fretted terrain formed (*Irwin et al., 2004*). This reactivation likely consisted of multiple flow episodes of similar magnitudes, as inferred from the lack of trenching or incision of the front scarps of the two deltas. The relationship with the fretted terrains indicates that the incision occurred during or after the early Hesperian epoch.

The sinuous ridges found within Robert Sharp crater (Fig. 6d) are interpreted as inverted channels, formed after inversion of the relief by differential erosion. Due to the lack of clear evidence for glacial activity in the crater it seems unlikely that these sinuous ridges are subglacial eskers. They are morphologically similar to those seen in Gale and they present a consistent downslope orientation which corroborates the idea that those features represent an older aqueous drainage pattern (e.g., *Anderson and Bell, 2010; Le Deit et al., 2013; Palucis et al., 2014*).

The two fan-shaped deposits have a morphology and topography characteristic of single scarped, smooth, prograding deltas; with flat-topped surfaces and distal margins clearly marked by steep frontal scarps (e.g., *Irwin et al., 2005; deVilliers et al., 2013*). Deltas display a steep peripheral scarp at their outer margin, a genetic distinction that contrasts with the slightly concave longitudinal profile of alluvial fans (*Moore and Howard, 2005*). Such deltas usually result from a river encountering a stagnant body of water (e.g., a lake), and would imply a lacustrine episode within Robert Sharp crater. The scarp crests on the two deltas occur at the same elevation (–2400 m), consistent with ponding in the western half of the Robert Sharp basin (Fig. 7). On the basis of our longitudinal profiles (Fig. 7), the front scarps are estimated to dip 6–11 degrees, consistent

with Gilbert-type deltas (*Gilbert, 1980; Nemec, 1990*). We suggest that Robert Sharp deltas may resemble terrestrial shallow fan deltas (*Galloway, 1976; Wescott and Ethride, 1990*). On Earth such deltas encroach onto low-gradient shelves with very shallow water depths near river mouths. The gently dipping part may have been the subaerial portion of the delta, while the more inclined part corresponds to the submerged delta front. Similar deltas are found on Mars, e.g., Pancake delta within Gale crater (*Palucis et al., 2016*), with an arcuate shape, a fairly well preserved delta front, and surface area of ~100 km^2. Considering that the floor of Robert Sharp crater lies at an elevation as low as around –2700 m, we can estimate a lake depth of about 100–300 m (in agreement with the ~200 m deep paleolake predicted by *Rivera-Hernández and Palucis, 2019*). Our crater counting predicts that both deltas have Amazonian ages, while the adjacent crater floor deposits have an older age close to the late Hesperian to early Amazonian transition (Fig. 8). The crater floor deposits are located topographically below the two deltas in Robert Sharp, and possibly stratigraphically lower (Fig. 9a). It is possible that they were deposited before the deltas, and more precisely, before the last lacustrine episode associated to the delta formation. They may correspond to draping deposits that have been buried by lacustrine deposits that formed at the outlet of the deltas and were later exhumed. If the draping deposits were not completely exhumed, some of the crater floor may still be lacustrine deposits (Fig. 9b).

Interestingly, Robert Sharp's sinuous ridges are seen on the crater floor deposits, indicating a possible channelization coeval to (or prior) the lacustrine episode within the crater. Then, the channels could have been buried by lacustrine deposits. Finally, their exhumation and subsequent segmentation by aeolian abrasion started after the lake disappearance, and still continues nowadays.

5.4 Polygonal ridges

Polygonal ridges within Robert Sharp have morphologies indicating an origin by mineralization of fractures. Such ridges are interpreted as fractures filled and cemented by minerals that were precipitated from near-surface groundwater (e.g., *Thomson et al., 2011; Kerber et al., 2017*). *Kerber et al. (2017)* classified Robert Sharp ridges as 'Nili-type' ridges. They consist of mostly light-toned ridges of varying thickness intersecting at a wide variety of angles, like most polygonal ridges described in the Nili Fossae and Nilosyrtis regions (*Ebinger and Mustard, 2015; Kerber et al., 2017; Pascuzzo et al., 2019*). Similar features are seen within Gale and,

more precisely, were found at the basis of Aeolis Mons (*Anderson and Bell, 2010; Thomson et al., 2011; Siebach and Grotzinger, 2014; Kronyak et al., 2019*), and in the eastern part of Gale (*Le Deit et al., 2013*). Polygonal ridges in Robert Sharp show similarities with polygonal ridges in Gale in terms of morphology, but not in size. Gale's polygonal ridges are smaller than those in Robert Sharp and are tens of meters long (e.g., *Le Deit et al., 2013*). In Gale, they have been attributed to the preferential cementation of material due to the circulation of fluids through fracture systems (*Thomson et al., 2011; Kerber et al., 2017*). The morphological similarities between Gale's polygonal ridges and those identified in Robert Sharp (Nili-type ridges) suggest that Gale's polygonal ridges are simply smaller versions of Nili-types. These polygonal ridges are indicative of fluid circulation within the fretted terrain and the draping materials that may be coeval to the late lacustrine phase in Robert Sharp crater.

6 Robert Sharp's mineralogy

Several mineral types have been detected in Robert Sharp crater and surroundings (Fig. 10). *Ehlmann and Buz (2015)* detected Fe/Mg smectites in the southwest fan delta, the most common hydrated minerals found on Mars (*Carter et al., 2013*). Their infrared signature displays spectral absorption bands at 1.4, 1.9 and 2.3 μm, which is consistent with a composition intermediate between end-member smectites nontronite (Fe-rich) and saponite (Mg-rich) (*Viviano-Beck et al., 2014; 2015*). They appear in light-toned layered deposits along the delta front and at its foot (*Ehlmann and Buz, 2015*, Figs. 10d–e). Fe/Mg clay minerals may be authigenic and have formed either during the transport of sediment or within the lake itself. Alternatively, they may be detrital and have formed upstream by near-surface weathering and were subsequently transported and deposited in the fan. This latter hypothesis is supported by the occurrence of clays exposed along the channel incising the southern wall of the crater and on the perched plateau associated with chlorides (*Osterloo et al., 2008, 2010; Ruesch et al., 2012*). In addition to Fe/Mg smectites, *Ehlmann and Buz (2015)* found Al smectites (montmorillonite, kaolinite), or possibly hydrated silica locally in the southwest delta, with typical spectral absorption bands at 1.4, 1.9 and 2.2 μm. Hydrated silica is commonly observed on fan deltas on Mars, and may have formed in-situ through chemical alteration during surface water flow and ponding (e.g., *Carter et al., 2012; Hauber et al., 2013; Pan et al., 2019; Pineau et al., 2020*). Al smectites may have formed in

deltaic environments by weathering. This formation process has also been proposed for a delta located at the dichotomy boundary in Lybia Montes (*Erkeling et al., 2012; 2015*).

Other hydrated minerals within Robert Sharp such as akaganeite and Fe carbonates (siderite) were reported by *Carter et al. (2015)*. Akaganeite (β–FeOOH, Cl) is an iron chlorine hydroxide that is associated on Earth to acidic and oxidizing conditions in a drying lake or lagoon (*Bibi et al., 2011*). Akaganeite occurs systematically in small depressions in Robert Sharp (Figs. 10f–g), which correspond to possible late stage ponding locations. Similar deposits are found in localized topographic lows in Jezero crater and northeast Syrtis (*Dundar et al., under review*).

Thanks to the analysis of the CRISM multispectral data, we found mixtures of Fe/Mg smectites, Al smectites (or hydrated silica), and sulfates in close proximity to the polygonal ridges lying on the draping deposits (Fig. 10h). This is likely related to mineral cementation associated with diagenesis in sediments, like in Gale (*Siebach and Grotzinger, 2014*). Additionally, the geometry and characteristics of the polygonal ridges as well as the presence of sulfates support the idea that the ridges are formed by chemical alteration or precipitation of minerals in or along pre-existing fractures. Sulfate salts can precipitate during alteration by circulating groundwater (*Andrews-Hanna and Lewis, 2011*), as suggested in Gale crater (*Grotzinger et al., 2014; 2015; Siebach and Grotzinger, 2014*). Other examples of filled fractured networks present in sulfate-bearing deposits were reported in Candor Chasma (*Okubo and McEwen, 2007*) and northeast Syrtis Major (*Ehlmann and Mustard, 2012*). However, our newly detected mixtures of smectites and sulfates within Robert Sharp are found in an area of the crater covered by dust (Fig. 2d) and that is only observed through CRISM data at low spatial resolution (~200 m per pixel) and low spectral resolution (~50 nm per channel) (*Murchie et al., 2007; Pelkey et al., 2007*). Thus, these detections are less robust than the previous ones obtained with CRISM data at scales of ~18 m per pixel and spectral resolutions of 6.55 nm per channel.

[Figure 10]

7 Robert Sharp's geological history

After its formation between the middle Noachian and early Hesperian epoch (Fig. 11a), Robert Sharp has experienced an infilling stage with sedimentary and/or volcano-sedimentary material during the early Hesperian (Fig. 11b). Subsequently, this material underwent a significant

458 degradation, leading to the fretted terrain formation during the early Hesperian epoch. The crater
459 floor is therefore predominantly dotted with mesas and knobs (Fig. 11c). Later, the draping
460 deposits have partially or entirely filled the crater as well as the surrounding plateaus to the east
461 of Robert Sharp through airfall/aeolian deposition of fine-grained sediment like dust and/or
462 volcanic ash (Fig. 11d). These deposits are not found in the western floor of the crater and it is
463 difficult to determine whether they once filled the western side of the crater or not. Fluvial
464 activity leads to the incision of the western and southwestern walls of Robert Sharp and carried
465 sedimentary material within the crater. Then, the fan-shaped deposits and the crater floor
466 deposits record lacustrine episodes filling the lower parts of the crater between the Hesperian and
467 early Amazonian epoch (Fig. 11e). The fretted terrain and draping deposits might have been
468 exposed over a broader area in the crater during the Hesperian epoch, and then removed by late
469 fluvial and aeolian degradation in the western part of the crater. The deltas and chloride-rich
470 deposits show model ages of ~1 Ga to hundreds of Ma (Fig. 8), but due to the small counting
471 areas and the possibility of removal of the oldest craters, our ages may be underestimated (e.g.,
472 *von der Bogert et al., 2015; Warner et al., 2015; Palucis et al., 2020*). However, stratigraphic
473 relationships were taken into account when existing, and they show that the deltas and chloride-
474 basin are younger than the underlying materials, hence implying a formation during the
475 Hesperian or after. Afterwards, this activity becomes progressively more spatially localized and
476 episodic in the Hesperian – Amazonian period, with deposition of the chloride-rich material in
477 local depressions and remobilization of Fe/Mg phyllosilicates in deltas. Finally, after the
478 disappearing of the lake, the crater floor exhibits a plethora of mineral phases suggesting diverse
479 environmental conditions (Fig. 11f), from neutral, reducing to mildly acidic, highly saline and
480 oxidizing conditions.

481 [Figure 11]

482 **8 Implications of aqueous activity for the Robert Sharp and Gale craters region**

483 Like Robert Sharp, Gale exhibits several morphologic features suggestive of fluvial, deltaic and
484 lacustrine processes in its interior, notably the presence of well-defined valleys incising the crater
485 from the west and south, and fan-shaped deposits resembling deltas at their termini (e.g.,
486 *Anderson and Bell, 2010; Le Deit et al., 2013; Palucis et al., 2014; 2016*). Deltas in the western
487 half of Gale suggest a series of lake stands postdating the formation of the layered mound –

Aeolis Mons – in the Hesperian epoch (*Le Deit et al., 2013; Grant et al., 2014; Palucis et al., 2016*). They show evidence of late resurfacing during the Hesperian and possibly Amazonian epochs (*Grant et al., 2014; 2019; Palucis et al., 2014*), and therefore yield ages broadly comparable to those obtained for the two deltas in Robert Sharp (Fig. 8, also in *Ehlmann and Buz, 2015*). This could indicate a contemporaneous aqueous phase in both Robert Sharp and Gale craters. Moreover, recent K-Ar dating of a mudstone and a sandstone in Gale performed by the Curiosity rover yield an Amazonian (<3.0 Ga) bulk age (*Martin et al., 2017*). Large-scale fluvial activity on Mars is thought to have ceased by the early Hesperian (*Irwin et al., 2005; Fassett and Head, 2008*), though fluvio-deltaic activity possibly continued during the early – middle Amazonian period near the two craters (*Hauber et al., 2013*). By contrast, the Murray formation at the base of Aeolis Mons in Gale corresponds to lacustrine sandstones and mudstones that were emplaced before the formation and degradation of Aeolis Mons in its current morphology (*Stein et al., 2018; Stack et al., 2019*). Hence, Gale underwent another, older lacustrine phase prior to 3.3–3.1 Ga in the Hesperian epoch (*Grant et al., 2014; Grotzinger et al., 2015*). The crater floor deposits currently exposed in Robert Sharp crater may record a similar lacustrine phase. However, orbital data alone do not allow to decipher the sedimentary facies and lithology of the rocks forming the crater floor deposits.

Orbital detection of akaganeite mixed with Fe carbonates within Robert Sharp suggests acidic, chlorinated and oxidizing conditions during a lacustrine phase (*Carter et al., 2015*). Interestingly, akaganeite was detected as a minor phase in mudstone samples drilled by Curiosity rover within Gale (in Yellowknife Bay, *Ming et al., 2014; Vaniman et al., 2014*). However, the presence of Ca sulfates and magnetite and the lack of Fe sulfates within those samples indicate a quasi-neutral and poorly saline environment during this aquatic phase of Gale (*Grotzinger et al., 2014; 2015*). The existence of these two contrasting environmental conditions has been later supported by recent experimental works (*Peretyazhko et al., 2018*). Robert Sharp and Gale craters may have undergone different geochemical environments through time.

9 Conclusion

Our findings reveal that Robert Sharp was shaped by a variety of geological processes of different nature, such as fretted terrain formation, airfall deposition, fluvial, deltaic and lacustrine phase(s), and chemical precipitation. After the impact that formed the crater near the middle

Noachian and early Hesperian epoch (*Tanaka, 1986*), Robert Sharp experienced the deposition and erosion of the fretted terrain, followed by the airfall deposition draping previous formations during the Hesperian epoch (*Irwin et al., 2004; Irwin and Watters, 2010*). The presence of fluvial valleys and fan deltas as well as hydrous minerals within the crater and on its watershed, suggests a history of past fluviolacustrine activity throughout the region. The detection of akaganeite, a mineral with very specific formation conditions (*Carter et al., 2015; Peretyazhko et al., 2018*), indicates that Robert Sharp has experienced a mildly acidic, highly saline and oxidizing environment during the last alteration phase of a drying lake. The fluviolacustrine phase is likely related to the aqueous activity that formed the chloride-rich deposits on the neighboring plateaus (*Osterloo et al., 2008, 2010, Ruesch et al., 2012*), as well as the deltas. The last episodes of aqueous activity may be as recent as the early – middle Amazonian period, between 1.43 Ga and 512 Ma. As demonstrated with Robert Sharp, the region is shown to have experienced several episodes of aqueous activity well after the late Noachian – early Hesperian boundary, probably extending to the middle Amazonian epoch.

Acknowledgements

We greatly thank the THEMIS, HRSC, CTX, HiRISE and MOLA teams responsible for the orbital data used in the study. All data used in the work are publicly available through the NASA Planetary Data System (PDS) Imaging Node portal (http://pds-imaging.jpl.nasa.gov/portal). We also thank our two anonymous reviewers for their thoughtful and thorough comments that significantly improved the manuscript.

References

Amidon, W.H., Clark, A.C., 2015. Interaction of outburst floods with basaltic aquifers on the Snake River Plain: Implications for Martian canyons. GSA Bull. 127, 688–701. https://doi.org/10.1130/B31141.1

Anderson, R.B., Bell, J.F., 2010. Geologic mapping and characterization of Gale Crater and implications for its potential as a Mars Science Laboratory landing site. Mars 5, 76–128. https://dx.doi.org/10.1555/mars.2010.0004

545 Andrews-Hanna, J.C., Lewis K.W., 2011. Early Mars hydrology 2: Hydrological evolution in the
546 Noachian and Hesperian epochs. JGR 116, E02007. https://doi.org/10.1029/2010JE003709

547 Baker, V.R., et al., 2015. Fluvial geomorphology on Earth-like planetary surfaces: A review.
548 Geomorphology 245, 149–182. http://dx.doi.org/10.1016/j.geomorph.2015.05.002

549 Bibi, I., Singh, B., Silvester, E., 2011. Akaganeite (β-FeOOH) precipitation in inland acid sulfate
550 soils of south-western New South Wales (NSW), Australia. Geochim. Cosmochim. Acta 75,
551 6429–6438. https://doi.org/10.1016/j.gca.2011.08.019

552 Bibring, J.-P., et al., 2005. Mars surface diversity as revealed by the OMEGA/Mars Express
553 observations. Science 307, 1576–1581. https://doi.org/10.1126/science.1108806

554 Breed, C.S., McCauley, J.F., Grolier, M.J., 1982. Relict drainages, conical hills, and the eolian
555 veneer in southwest Egypt – Applications to Mars. JGR 87 (B12), 9929–9950.
556 https://doi.org/10.1029/JB087iB12p09929

557 Carr, M.H., 1995. The Martian drainage system and the origin of valley networks and fretted
558 channels. JGR 100 (E4), 7479–7507. https://doi.org/10.1029/95JE00260

559 Carr, M.H., 1996. Water on Mars. Oxford University Press, Oxford (229 pages).

560 Carter, J., et al., 2012. Composition of alluvial fans and deltas on Mars. 43rd LPSC Abstracts, p.
561 2.

562 Carter, J., Poulet, F., Bibring, J.-P., Mangold, N., Murchie, S., 2013. Hydrous minerals on Mars
563 as seen by the CRISM and OMEGA imaging spectrometers: Updated global view. JGR 118,
564 831–858. https://doi.org/10.1029/2012JE004145

565 Carter, J., Viviano-Beck, C., Loizeau, Bishop, J., Le Deit, L., 2015. Orbital detection and
566 implications of akaganeite on Mars. Icarus 253, 296–310.
567 http://dx.doi.org/10.1016/j.icarus.2015.01.020

568 Christensen, P.R., et al., 2004. The thermal emission imaging system (THEMIS) for the Mars
569 2001 Odyssey mission. SSR 110 (1-2), 85–130. https://doi.org/10.1007/978-0-306-48600-5_3

570 Denton, C.A., Head, J.W., 2018. Mapping the fretted terrain north of Arabia Terra, Mars: Results
571 and implications for dichotomy boundary evolution. 49th LPSC Abstracts, 1597.

572 De Villiers, G., Kleinhans, M.G., Postma, G., 2013. Experimental delta formation in crater lakes
573 and implications for interpretation of Martian deltas. JGR 118, 651–670.
574 https://doi.org/10.1002/jgre.20069

575 Dundar, M., Ehlmann, B. L., Leask, E.K., (year?). Machine-learning-driven new geologic
576 discoveries at Mars rover landing sites: Jezero and NE Syrtis. GRL (under review).
577 https://doi.org/10.1002/essoar.10501294.1

578 Ebinger, E.K., Mustard, J.F., 2015. Linear ridges in the Nilosyrtis region of Mars: Implications
579 for subsurface fluid flow. 46th LPSC Abstracts, 2034.

580 Ehlmann, B.L., Buz, J., 2015. Mineralogy and fluvial history of the watersheds of Gale, Knobel,
581 and Sharp craters: A regional context for the Mars Science Laboratory Curiosity's exploration.
582 GRL 42, 264–273. http://dx.doi.org/10.1002/2014GL062553

583 Erkeling, G., et al., 2012. Valleys, paleolakes and possible shorelines at the Libya Montes/Isidis
584 boundary: implications for the hydrologic evolution of Mars. Icarus 219, 393–413.
585 https://doi.org/10.1016/j.icarus.2012.03.012

586 Erkeling, G., et al., 2015. Valleys, fan-shaped deposits and associated Phyllosilicates of a
587 Paleolake site at Libya Montes, Mars: evidence of complex hydrologic activity. 46th LPSC
588 Abstracts, p. 1779.

589 Fassett, C.I., Head, J.W., 2007. Layered mantling deposits in northeast Arabia Terra, Mars:
590 Noachian- Hesperian sedimentation, erosion, and terrain inversion. JGR 112 (E08002).
591 http://dx.doi.org/10.1029/2006JE002875

592 Fassett, C.I., Head, J.W., 2008. The timing of Martian valley network activity: Constaints from
593 buffered crater counting. Icarus 195, 61–89. https://doi.org/10.1016/j.icarus.2007.12.009

594 Fedo, C.M., et al., 2019. Evidence for persistent, water-rich, lacustrine deposition preserved in
595 the Murray formation, Gale crater: A depositional system suitable for sustained habitability. In
596 the 9th International Conference on Mars, 2089.

597 Fergason, R.L., Christensen, P.R., Kieffer, H.H., 2006. High-resolution thermal inertia derived
598 from the Thermal Emission Imaging System (THEMIS): Thermal model and applications. JGR
599 111, E12004. http://dx.doi.org/10.1029/2006JE002735

600 Galloway, W.E., 1976. Sediments and stratigraphic framework of the Copper River fan delta,
601 Alaska. J. Sediment. Petrol. 49, 726–737. https://doi.org/10.1306/212F703B-2B24-11D7-
602 8648000102C1865D

603 Gilbert, G.K., 1980. Lake Bonneville, U.S. Geological Survey Monograph, Vol. 1 (438 pages).

604 Glotch, T.D., Kraft, M.D., 2008. Thermal transformation of akaganeite and lepidocrocite to
605 hematite: assessment of possible precursors to Martian crystalline hematite. Phys. Chem.
606 Minerals (35), 569–581. https://doi.org/10.1007/s00269-008-0249-z

607 Grant, J.A., Wilson, S.A., Mangold, N., Calef III, F., Grotzinger, J.P., 2014. The timing of
608 alluvial activity in Gale crater, Mars. GRL 41, 1142–1148.
609 https://dx.doi.org/10.1002/2013GL058909

610 Grant, J.A., Wilson, S.A., 2019. Evidence for late alluvial activity in Gale Crater, Mars. GRL 46,
611 7287–7294. https://doi.org/10.1029/2019GL083444

612 Grotzinger, J.P., and MSL Science Team, 2014. A habitable fluvio-lacustrine environment at
613 Yellowknife Bay, Gale Crater, Mars. Science 343. https://dx.doi.org/10.1126/science.1242777

614 Grotzinger, J.P., and MSL Science Team, 2015. Deposition, exhumation, and paleoclimate of an
615 ancient lake deposit, Gale crater, Mars. Science 350. https://dx.doi.org/10.1126/science.aac7575

616 Gwinner, K., et al., 2010. Topography of Mars from global mapping by HRSC high-resolution
617 digital terrain models and orthoimages: Characteristics and performance. EPSL 294, 506–519.
618 http://dx.doi.org/10.1016/j.epsl.2009.11.007

619 Hamilton, E., Osterloo, M.M., McGrane, B.S., 2007. THEMIS Decorrelation Stretched infrared
620 mosaics of candidate 2009 Mars Science Laboratory landing sites: Evidence for significant
621 spectral diversity. 40th LPSC Abstracts, p. 1725.

622 Harrison, K.P., Grimm, R.E., 2005. Groundwater-controlled valley networks and the decline of
623 surface runoff on early Mars. JGR 110, E12S16. https://doi.org/10.1029/2005JE002455

624 Hartmann, W.K., Neukum, G., 2001. Cratering chronology and the evolution of Mars. SSR 96,
625 165–194. https://doi.org/10.1023/A:1011945222010

626 Hauber, E., et al., 2013. Asynchronous formation of Hesperian and Amazonian-aged deltas on
627 Mars and implications for climate. JGR 118 (7), 1529–1544.
628 http://dx.doi.org/10.1002/jgre.20107

629 Head, J.W., Kreslavsky, M., 2004. Medusae Fossae Formation: Ice-rich airborne dust deposited
630 during periods of high obliquity? 35th LPSC Abstracts, p. 1636.

631 Howard, A.D., McLane, C.F., 1988. Erosion of cohesionless sediment by groundwater seepage.
632 Water Resources Research 24 (10), 1659–1674. https://doi.org/10.1029/WR024i010p01659

633 Irwin, R.P., Howard, A.D., 2002. Drainage basin evolution in Noachian Terra Cimmeria, Mars.
634 JGR 107 (E7). https://doi.org/10.1029/2001JE001818

635 Irwin, R.P., Watters, T.R., Howard, A.D., Zimbelman, J.R., 2004. Sedimentary resurfacing and
636 fretted terrain development along the crustal dichotomy boundary, Aeolis Mensae, Mars. JGR
637 109 (E09011). http://dx.doi.org/10.1029/2004JE002248

638 Irwin, R.P., Howard, A.D., Craddock, R.A., Moore, J.M., 2005. An intense terminal epoch of
639 widespread fluvial activity on early Mars: 2. Increased runoff and paleolake development. JGR
640 110 (E12). https://doi.org/10.1029/2005JE002460

641 Irwin, R.P., Watters, T.R., 2010. Geology of the Martian crustal dichotomy boundary: Age,
642 modifications, and implications for modeling efforts. JGR 115 (E11006).
643 http://dx.doi.org/10.1029/2010JE003658

644 Ivanov, B.A., 2001. Mars/Moon cratering rate ratio estimates. SSR 96, 87–124.
645 https://doi.org/10.1023/A:1011941121102

Jaumann, R., et al., 2007. The High-Resolution Stereo Camera (HRSC) experiment on Mars Express: Instrument aspects and experiment conduct from interplanetary cruise through the nominal mission. PSS 55, 928–952. https://doi.org/10.1016/j.pss.2006.12.003

Kerber, L., et al., 2011. The dispersal of pyroclasts from Apollinaris Patera, Mars: Implications for the origin of the Medusae Fossae Formation. Icarus 216, 212–220. https://doi.org/10.1016/j.icarus.2011.07.035

Kerber, L., Dickson, J.L., Head, J.W., Grosfils, E.B., 2017. Polygonal ridge networks on Mars: Diversity of morphologies and the special case of the Eastern Medusae Fossae Formation. Icarus 281, 200–219. http://dx.doi.org/10.1016/j.icarus.2016.08.020

Kneissl, T., van Gasselt, S., Neukum, G., 2011. Map-projection-independent crater size-frequency determination in GIS environments – New software tool for ArcGIS. PSS 59, 1243–1254. https://doi.org/10.1016/j.pss.2010.03.015

Kronyak, R.E., et al., 2019. Extensive polygonal fracture network in Siccar point group strata: Fracture mechanisms and implications for fluid circulation in Gale crater, Mars. JGR 124, 2613–2634. https://doi.org/10.1029/2019JE006125

Lamb, M.P., et al., 2006. Can springs cut canyons into rock? JGR 111, E07002. https://doi.org/10.1029/2005JE002663

Lapotre, M.G., Lamb, M.P., 2018. Substrate controls on valley formation by groundwater on Earth and Mars. Geology 46 (6), 531–534. https://doi.org/10.1130/G40007.1

Le Deit, L., Hauber, E., Fueten, F., Pondrelli, M., Rossi, A.P., Jaumann, R., 2013. Sequence of infilling events in Gale crater, Mars: Results from morphology, stratigraphy, and mineralogy. JGR 118 (12), 2439–2473. http://dx.doi.org/10.1002/2012JE004322

Malin, M.C., et al., 2007. Context camera investigation on board the Mars Reconnaissance Orbiter. JGR 112 (E05). http://dx.doi.org/10.1029/2006JE002808

Mandt, K.E., de Silva, S.L., Zimbelman, J.R., Crown, D. A., 2008. Origin of the Medusae Fossae Formation, Mars: Insights from a synoptic approach. JGR 113, E12011. https://doi.org/10.1029/2008JE003076

673 Mangold, N., 2005. High latitude patterned grounds on Mars: Classification, distribution and
674 climatic control. Icarus 174 (2), 336–359. Mars Polar Science {III}.
675 http://dx.doi.org/10.1016/j.icarus.2004.07.030

676 Mangold, N., et al., 2012. The origin and timing of fluvial activity at Eberswalde crater, Mars.
677 Icarus 220 (2), 530–551. https://doi.org/10.1016/j.icarus.2012.05.026

678 Marra. W.A., Braat, L., Baar, A.W., Kleinhans, M.G., 2014. Valley formation by groundwater
679 seepage, pressurized groundwater outbursts and crater-lake overflow in flume experiments with
680 implications for Mars. Icarus 232, 97–117. http://dx.doi.org/10.1016/j.icarus.2013.12.026

681 Martin, P.E., et al., 2017. A two-step experiment on Mars: Dating the diagenetic formation of
682 jarosite from Amazonian groundwaters. JGR 122, 2803–2818.
683 https://doi.org/10.1002/2017JE005445

684 Maxwell, T.A., McGill, G.E., 1988. Ages of fracturing and resurfacing in the Amenthes region,
685 Mars. LPSC Proceedings, 701–711.

686 McEwen, A.S., et al., 2007. Mars Reconnaissance Orbiter's High Resolution Imaging Sciences
687 Experiment (HiRISE). JGR 112, E05S02. http://dx.doi.org/10.1029/2005JE002605

688 McGill, G.E., 2000. Crustal history of north central Arabia Terra, Mars. JGR 105 (E3), 6945–
689 6959. https://doi.org/10.1029/1999JE001175

690 Michael, G., 2013. Planetary surface dating from crater size-frequency distribution
691 measurements: Multiple resurfacing episodes and differential Isochron fitting. Icarus 226, 885–
692 890. https://doi.org/10.1016/j.icarus.2013.07.004

693 Michael., G., Neukum, G., 2010. Planetary surface dating from crater size-frequency distribution
694 measurements: Partial resurfacing events and statistical age uncertainty. EPSL 294, 223–229.
695 https://doi.org/10.1016/j.epsl.2009.12.041

696 Ming, D.W., and MSL Science Team, 2014. Volatile and organic compositions of sedimentary
697 rocks in Yellowknife Bay, Gale crater, Mars. Science 343 (6169).
698 http://dx.doi.org/10.1126/science.1245267

699 Moore, J.M., Howard, A.D., 2005. Large alluvial fans on Mars. JGR 110, E04005.
700 https://doi.org/10.1029/2004JE002352

701 Murchie, S., et al., 2007. Compact Reconnaissance Imaging Spectrometer for Mars (CRISM) on
702 Mars Reconnaissance Orbiter (MRO). JGR 112, E05S03. https://doi.org/10.1029/2006JE002682

703 Nemec, W., 1990. Aspects of sediment movement on steep delta slopes. In Coarse-grained deltas
704 edited by A. Colella and D. P. Prior, Spec. Publ. Int. Assoc. Sediment. 10, 29–73.
705 https://doi.org/10.1002/9781444303858.ch3

706 Neukum, G., Jaumann, R., 2004. HRSC: The high resolution stereo camera of Mars express. In
707 Mars Express: The Scientific Payload, vol. 1240, 17–35.

708 Ojha, L., Lewis, K., 2018. The density of the Medusae Fossae Formation: Implications for its
709 composition, origin, and importance in Martian history. JGR 123, 1368–1379.
710 https://doi.org/10.1029/2018JE005565

711 Okubo, C.H., McEwen, A.S., 2007. Fracture-controlled paleo-fluid flow in Candor Chasma,
712 Mars. Science 315, 983–985. https://doi.org/10.1126/science.1136855

713 Osterloo, M.M., et al., 2008. Chloride-bearing materials in the southern highlands of Mars.
714 Science 319, 1651–1654. https://dx.doi.org/10.1126/science.1150690

715 Osterloo, M.M., Anderson, F.S., Hamilton, V.E., Hynek, B.M., 2010. Geologic context of
716 proposed chloride-bearing materials on Mars. JGR 115 (E10).
717 http://dx.doi.org/10.1029/2010JE003613

718 Palucis, M.C., et al., 2014. The origin and evolution of the Peace Vallis fan system that drains to
719 the Curiosity landing area, Gale Crater, Mars. JGR 119, 705–728.
720 https://dx.doi.org/10.1002/2013JE004583

721 Palucis, M.C., et al., 2016. Sequence and relative timing of large lakes in Gale crater (Mars) after
722 the formation of Mount Sharp. JGR 121, 472–496. https://dx.doi.org/10.1002/2015JE004905

723 Palucis, M.C., Jasper, J., Garczynski, B., Dietrich, W.E., 2020. Quantitative assessment of
724 uncertainties in modeled crater retention ages on Mars. Icarus 341, 113623.
725 https://doi.org/10.1016/j.icarus.2020.113623

Pan, L., Carter, J., Quantin-Nataf, C., 2019. Hydrated silica in Martian alluvial fans and deltas. 9th Internal Conference on Mars, p. 6239.

Pascuzzo, A.C., Mustard, J.F., Kremer, C.H., Ebinger, E., 2019. The formation of irregular polygonal ridge networks, Nili Fossae, Mars: Implications for extensive subsurface channelized fluid flow in the Noachian. Icarus 319, 852–868. https://doi.org/10.1016/j.icarus.2018.10.020

Pelkey, S.M., et al., 2007. CRISM multispectral summary products: Parameterizing mineral diversity on Mars from reflectance. JGR 112, E08S14. https://doi.org/10.1029/2006JE002831

Pelletier, J.D., Baker, V.R., 2011. The role of weathering in the formation of bedrock valleys on Earth and Mars: A numerical modeling investigation. JGR 116, E11007. https://doi.org/10.1029/2011JE003821

Peretyazhko, T.S., Ming, D.W., Rampe, E.B., Morris, R.V., Agresti, D.G., 2018. Effect of solution pH and chlorine concentration on akaganeite precipitation: Implications for akaganeite formation on Mars. JGR 123, 2211–2222. https://doi.org/10.1029/2018JE005630

Pineau, M., et al., 2020. Toward the geological significance of hydrated silica detected by near infrared spectroscopy on Mars based on terrestrial reference samples. Icarus, 113706. https://doi.org/10.1016/j.icarus.2020.113706

Pondrelli, M., et al., 2005. Complex evolution of paleolacustrine systems on Mars: An example from the Holden crater. JGR 110, E04016. https://doi.org/10.1029/2004JE002335

Rivera-Hernández, F., Palucis, M.C., 2019. Do deltas along the crustal dichotomy boundary of Mars in the Gale crater region record a northern ocean? GRL 46, 8689–8699. https://doi.org/10.1029/2019GL083046

Ruesch, O., et al., 2012. Compositional investigation of the proposed chloride-bearing materials on Mars using near-infrared orbital data from OMEGA/MEx. JGR 117 (E00J13). http://dx.doi.org/10.1029/2012JE004108

Ruff, S.W., Christensen, P.R., 2002. Bright and dark regions on Mars: Particle size and mineralogical characteristics based on Thermal Emission Spectrometer data. JGR 107 (E12), 5127. https://doi.org/10.1029/2001JE001580

753 Schultz, P.H., Lutz, A.B., 1988. Polar wandering of Mars. Icarus 73, 91–141.
754 https://doi.org/10.1016/0019-1035(88)90087-5

755 Scott, D.H., Tanaka, K.L., 1982. Ignimbrites of Amazonis Planitia Region of Mars. JGR 87,
756 1179–1190. https://doi.org/10.1029/JB087iB02p01179

757 Sharp, R.P., 1973. Fretted and Chaotic terrains. JGR 78 (20), 4073–4083.
758 https://doi.org/10.1029/JB078i020p04073

759 Sharp, R.P., Malin, M.C., 1975. Channels on Mars. GSA Bull. 86, 593–609.

760 Siebach, K.L., Grotzinger, J.P., 2014. Volumetric estimates of ancient water on mount Sharp
761 based on boxwork deposits, Gale crater, Mars. JGR 119 (1), 189–198.
762 http://dx.doi.org/10.1002/2013JE004508

763 Smith, D.E., et al., 2001. Mars Orbiter Laser Altimeter: Experiment summary after the first year
764 of global mapping of Mars. JGR 106, 23689–23722. http://dx.doi.org/10.1029/2000JE001364

765 Stack, K.M., et al., 2019. Evidence for plunging river plume deposits in the Pahrump Hills
766 member of the Murray formation, Gale crater, Mars. Sedimentology 66, 1768–1802.
767 https://doi.org/10.1111/sed.12558

768 Stein, N., et al., 2018. Desiccation cracks provide evidence of lake drying on Mars, Sutton Island
769 member, Murray formation, Gale Crater. Geology 46, 515–518.
770 https://doi.org/10.1130/G40005.1

771 Tanaka, K.L., 1986. The stratigraphy of Mars. Journal of Geophysical Research: Solid Earth 91
772 (B13), E139–E158. http://dx.doi.org/10.1029/JB091iB13p0E139

773 Tanaka, K.L., Robbins, S.J., Fortezzo, C.M., Skinner, J.A., Hare, T.M., 2014a. The digital global
774 geologic map of Mars: Chronostratigraphic ages, topographic and crater morphologic
775 characteristics, and updated resurfacing history. PSS 95, 11–24.
776 http://dx.doi.org/10.1016/j.pss.2013.03.006

777 Tanaka, K.L., et al., 2014b. Geologic map of Mars : U.S. Geological Survey Scientific
778 Investigations Map 3292, scale 1: 20,000,000. https://dx.doi.org/10.3133/sim3292

779 Thomson, B.J., Bridges, N.T., Milliken, R., et al., 2011. Constraints on the origin and evolution
780 of the layered mound in Gale crater, Mars using Mars Reconnaissance Orbiter data. Icarus 214
781 (2), 413–432. http://dx.doi.org/10.1016/j.icarus.2011.05.002

782 Vaniman, D.T., and MSL Science Team, 2014. Mineralogy of a mudstone at Yellowknife Bay,
783 Gale crater, Mars. Science 343 (6169). http://dx.doi.org/10.1126/science.1243480

784 Viviano-Beck, C.E., et al., 2014. Revised CRISM spectral parameters and summary products
785 based on the currently detected mineral diversity on Mars. JGR 119, 1403–1431.
786 https://doi.org/10.1002/2014JE004627

787 Viviano-Beck, C.E., et al., 2015. MRO CRISM type spectra library. NASA Planetary Data
788 System. http://crismtypespectra.rsl.wustl.edu

789 Von der Bogert, C.H., et al., 2015. Effects of count area size on absolute model ages derived
790 from random crater size-frequency distributions. 46th LPSC Abstracts, p. 1742.

791 Warner, N.H., et al., 2015. Minimum effective area for high resolution crater counting of
792 Martian terrains. Icarus 245, 198–240. http://dx.doi.org/10.1016/j.icarus.2014.09.024

793 Werner, S., Tanaka, K., 2011. Redefinition of the crater-density and absolute-age boundaries for
794 the chronostratigraphic system of Mars. Icarus 215 (2), 603–607. http://dx.doi.org/10.1016/j.
795 icarus.2011.07.024

796 Wescott, W.A., Ethridge, F.G., 1990. Fan deltas – alluvial fans in coastal settings. In Alluvial
797 fans : A field approach, edited by A. H. Rachocki and M. Church, 195–211, John Wiley,
798 Hoboken, N. J. https://doi.org/10.1306/2F918987-16CE-11D7-8645000102C1865D

Figures & Captions [2-column for all figures, and color should be used online only]

Fig. 1: Robert Sharp crater as seen through a mosaic of CTX images. Frames indicate the locations of the following figures; for the fretted terrains (yellow), draping deposits (brown), crater floor deposits (dark green), fluvial landforms (blue) and fan-shaped deposits (light green).

Fig. 2: Location and physiography of Robert Sharp. (a) MOLA DEM showing regional context of Robert Sharp and its two neighbors (Gale and Knobel craters) along the crustal dichotomy (isohypses every 200 m) (*Smith et al., 2001*). (b) MOLA DEM centered on Robert Sharp (isohypses every 200 m). (c) Qualitative thermal inertia ($J.m^{-2}.K^{-1}.s^{-1/2}$, *Fergason et al., 2006*) derived from THEMIS IR night-time (100 $m.px^{-1}$). (d) TES dust cover index (DCI) based on the emissivity value in the 1350–1400 cm^{-1} range (maximum dust at 0.9 and minimum dust at 1.0). The DCI is sensitive to the presence of silicate dust on the surface: orange and red colors indicate areas that likely are dust covered while blue areas likely are dust-free (*Ruff and Christensen, 2002*). The maps (a), (b) and (d) overlap a map from THEMIS IR day-time (100 $m.px^{-1}$).

Fig. 3: Morphologic map of Robert Sharp units defined as described in text, based on their location and physical properties such as surface texture, morphology, geometry and thermal inertia. Mesas and buttes from the fretted terrain (*Ft* unit, yellow), draping deposits that cover the eastern part of the basin and surrounding plateau (*Dp1–2* units, light and dark brown), crater floor deposits that lie flat on the western and southwestern parts of the basin (*Cf* unit, green), two fan-shaped deposits (*Fsd* unit, light blue) at the outlets of valley networks (cyan), and finally the sinuous ridges exposed on the crater floor (dark blue). The criteria used to distinguish the rough from smooth draping deposits (Dp1 and Dp2 units, respectively) are based on the texture aspect and brightness of the units in the CTX images (10-meter scale roughness). Locations of geological cross-sections in Fig. 4 are indicated.

Fig. 4: Geological cross-sections derived from MOLA DEM data: (a) west to east, (b) northwest to southeast and (c) southwest to northeast sections. The units are color-coded such as in the geological map of Robert Sharp (Fig. 3).

Fig. 5: (a) – (c) Mesas and knobs corresponding to the fretted terrains described in *Irwin et al. (2004)* and *Irwin and Watters (2010)*. (d) CTX image showing the draping units. (e) Close-up view of the contact between the Dp1 unit with a rough surface texture and the Dp2 unit with a

smoother appearance (HiRISE image, PSP_009360_1760_RED). (f) CTX image showing the draping deposits embaying and molding knobs and mesas. (g) Distribution of polygonal ridges (purple areas) found in Robert Sharp through a portion of CTX images. (h) Close-up view of a network of polygonal ridges (HiRISE image, ESP_042247_1760_RED).

Fig. 6: (a) Crater floor deposits. The isohypses – every 100 meters – reveal topographic basin in the mid-western floor of the crater. (b) – (c) Valleys found in the northwestern and southwestern walls of the crater, respectively. (d) Sinuous ridges embedded in the crater-floor deposits within Robert Sharp.

Fig. 7: (a) Northwestern (132.73°W, 3.6°S) and (b) southwestern (132.9°W, 5.1°S) fan-shaped deposits observed through CTX images. Topographic profile of (c) the northwestern and (d) the southwestern fan-shaped deposits (in light green) derived from the HRSC DEM with a vertical exaggeration of 5.6. The mean elevation at frontal scarp is about –2400 m for both deposits. Note that the morphology of both fan-shaped deposits appears broadly similar to the Pancake delta in Gale crater (*Palucis et al., 2016*).

Fig. 8: Age determination of surface units within and near Robert Sharp by crater-counting. (left) craters counted (in white) and the counting areas (in blue or green) on a mosaic of CTX images, except for (c) in a map THEMIS day-time. (right) crater size-frequency distribution that provide an inferred model age of the (a) southwestern and (b) northwestern fan-shaped deposits, (c) the crater floor deposits, and (d) the valley floor hosting the chloride-rich deposits (131°56'E, 6°25'S).

Fig. 9: (a) Simplified stratigraphic column for the main units within Robert Sharp. (b) Possible evolution of the crater floor based on the degradation of the lacustrine deposits (exhumation of the draping deposits).

Fig. 10: (a) Mars Orbiter Camera (MOC, 230 $m.px^{-1}$) map of Robert Sharp with spectral detections (color-coded) performed therein using the multispectral CRISM data. (b) MOC map of the southern perched plateau with detections in an enclosed basin: Fe/Mg smectites near chlorides (*Ruesch et al., 2012*). Chloride-rich deposits are indicated by the pink star, see also Fig. 3 (*Osterloo et al., 2008; 2010; Ruesch et al., 2012*). (c) to (h) show closer views of the spectral detections within the crater through CTX and HiRISE mages. (c) Fe/Mg smectites and Al

857 smectites (or hydrated silica) in delta fan (*Ehlmann and Buz, 2015*). They are observed as light-
858 toned layered deposits along the delta front and at its foot, white arrows in (d) and (e). (f) and (g)
859 show two sites of akaganeite with carbonates and Fe/Mg smectites located in small local
860 depressions (*Carter et al., 2015*). (h) shows a mixture of hydrated minerals on the draping
861 deposits and near polygonal ridges, with examples of spectra of hydrated minerals (mixtures)
862 detected on the draping deposits.

863 **Fig. 11:** Cartoon model illustrating the timing of geological events from the formation of Robert
864 Sharp to the present. (*) Age inferred by *Irwin et al. (2004)* and *Irwin and Watters (2010)*.

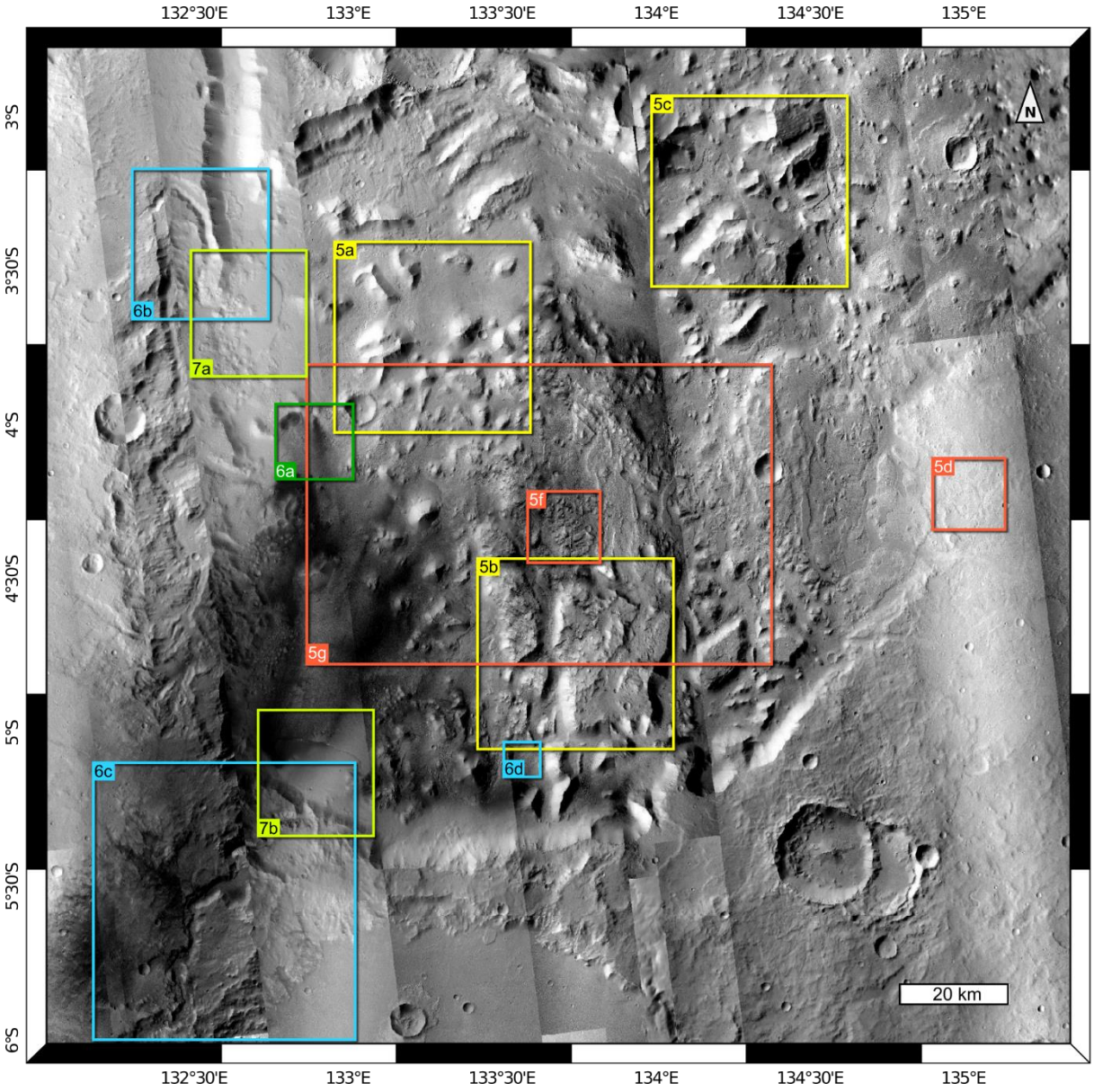
132°30'E
133°E
133°30'E
134°E
134°30'E
135°E
3°S
3°30'S
4°S
4°30'S
5°S
5°30'S
6°S
N
5c
5a
6b
7a
6a
5f
5d
5b
5g
6d
6c
7b
20 km

Figure 1

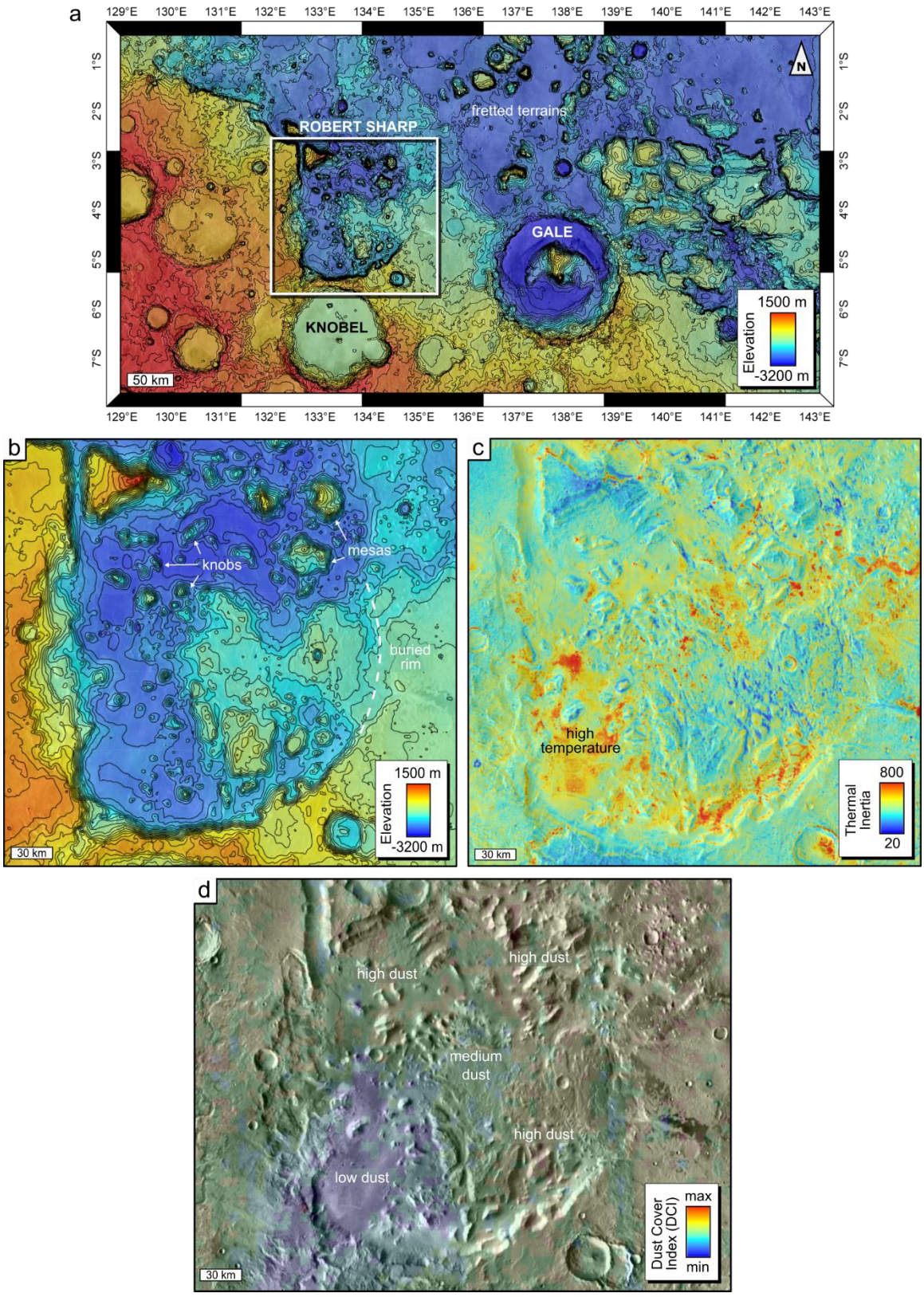

867

868 Figure 2

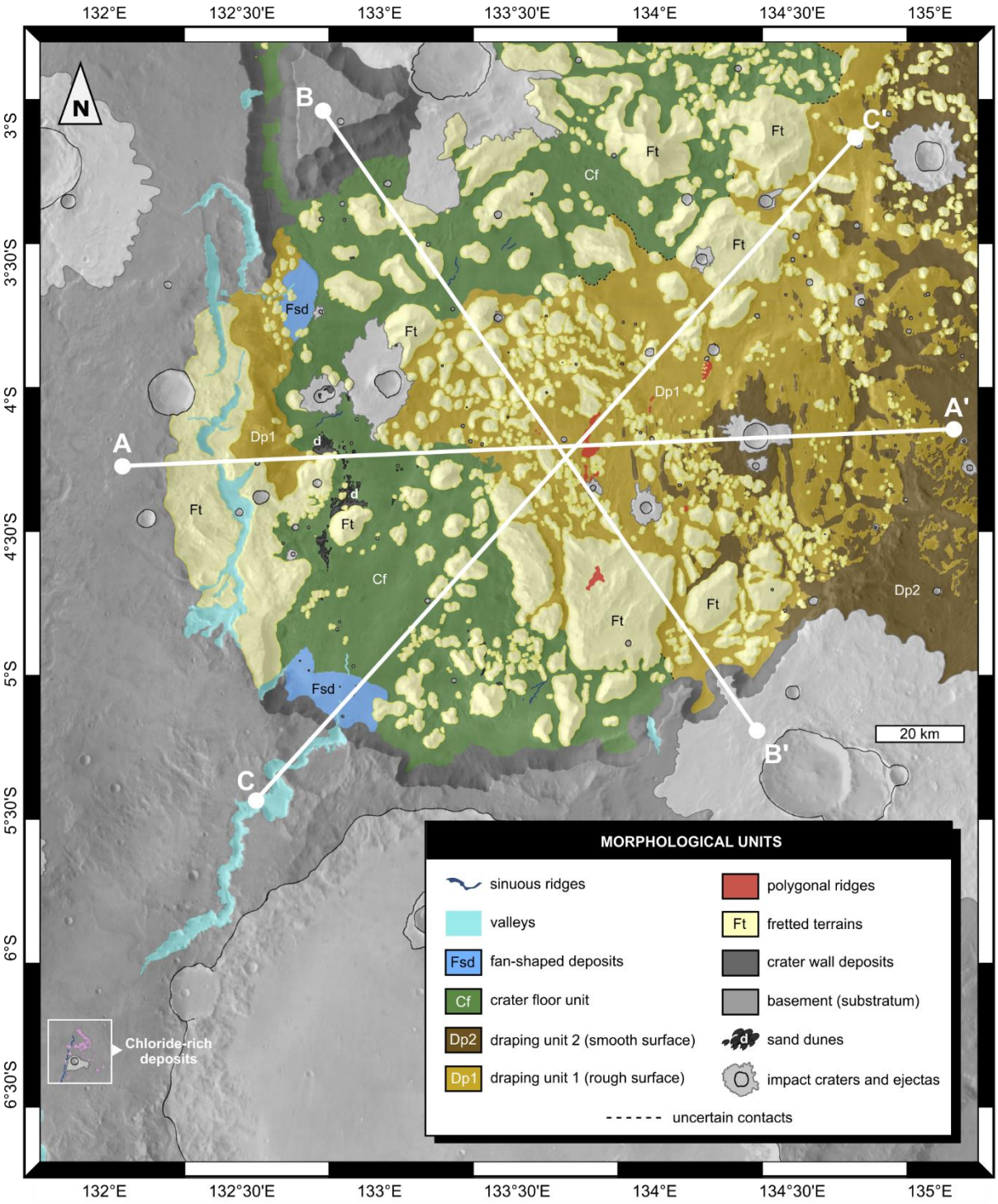

869

870 Figure 3

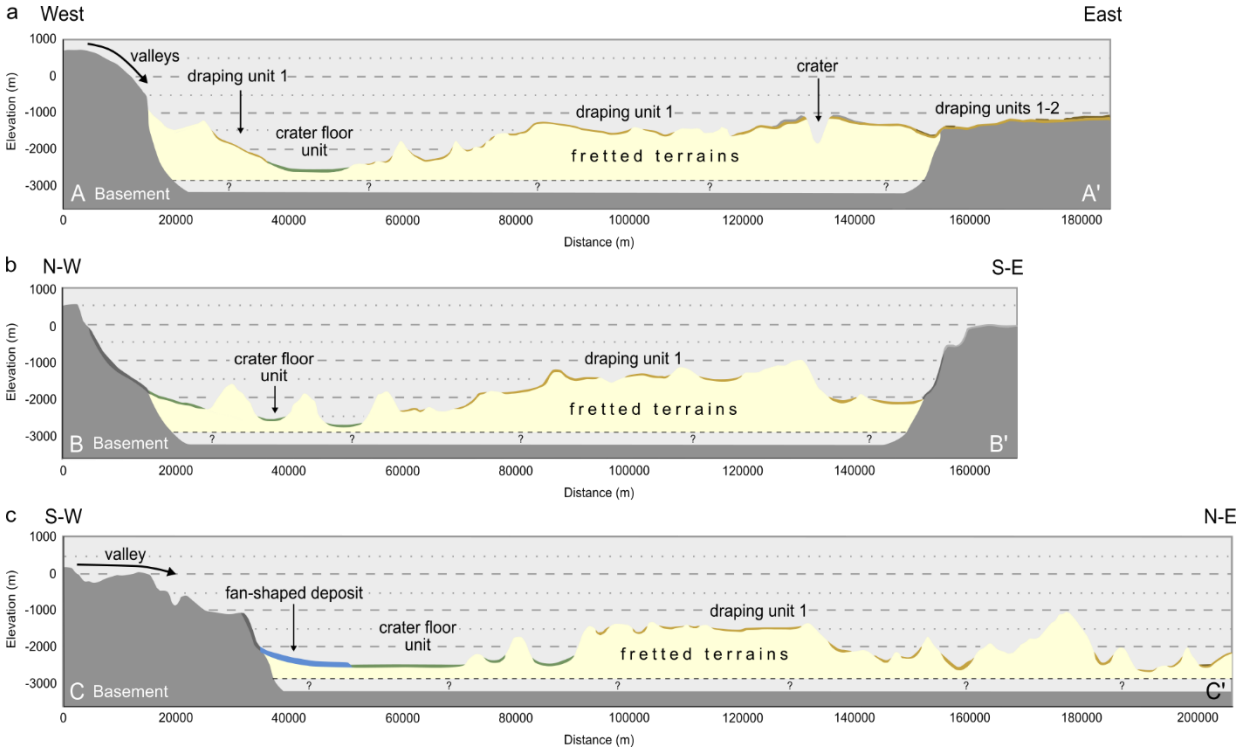
a
West
East
valleys
draping unit 1
crater
draping unit 1
draping units 1-2
crater floor unit
fretted terrains
A Basement
A'
Elevation (m)
Distance (m)
b
N-W
S-E
crater floor unit
draping unit 1
fretted terrains
B Basement
B'
c
S-W
N-E
valley
fan-shaped deposit
crater floor unit
draping unit 1
fretted terrains
C Basement
C'

Figure 4

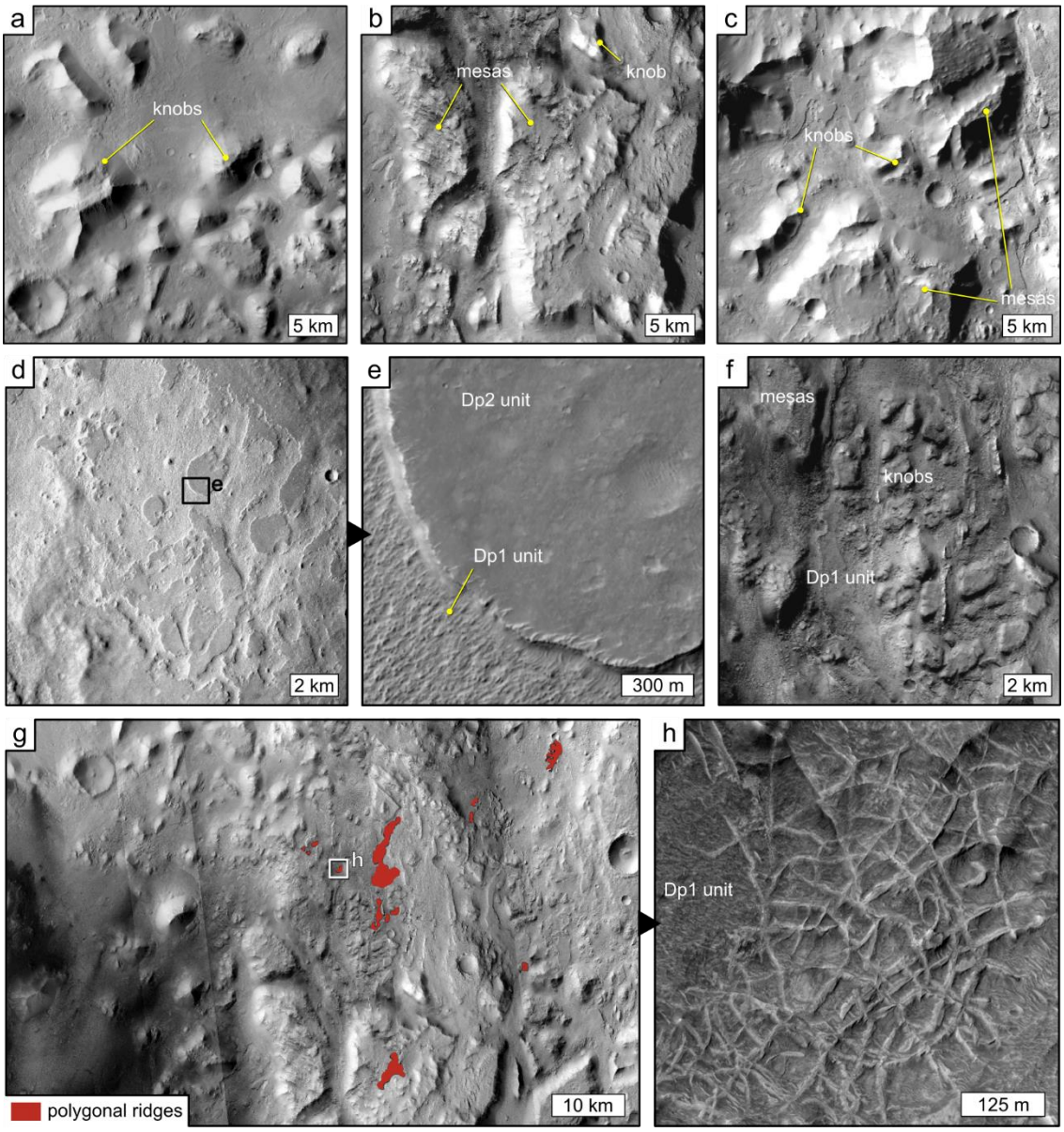

873

874 Figure 5

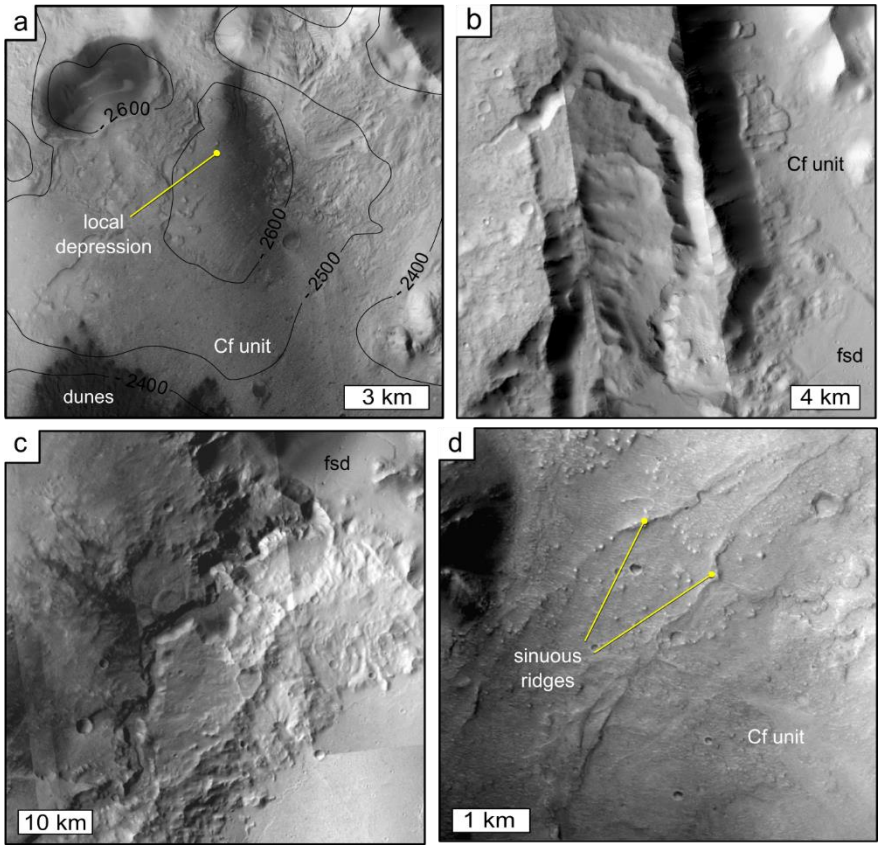

875

876 Figure 6

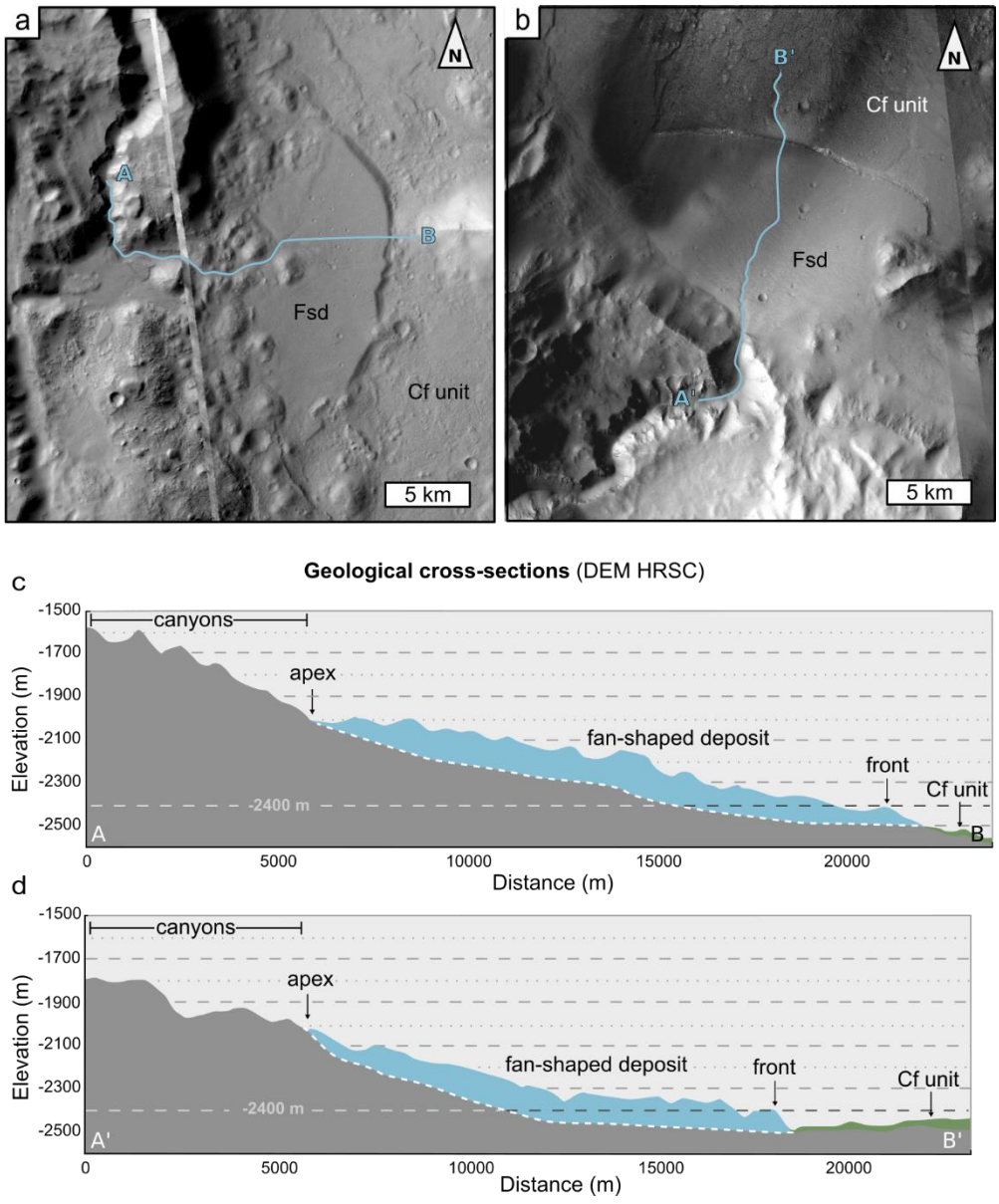

877

878 Figure 7

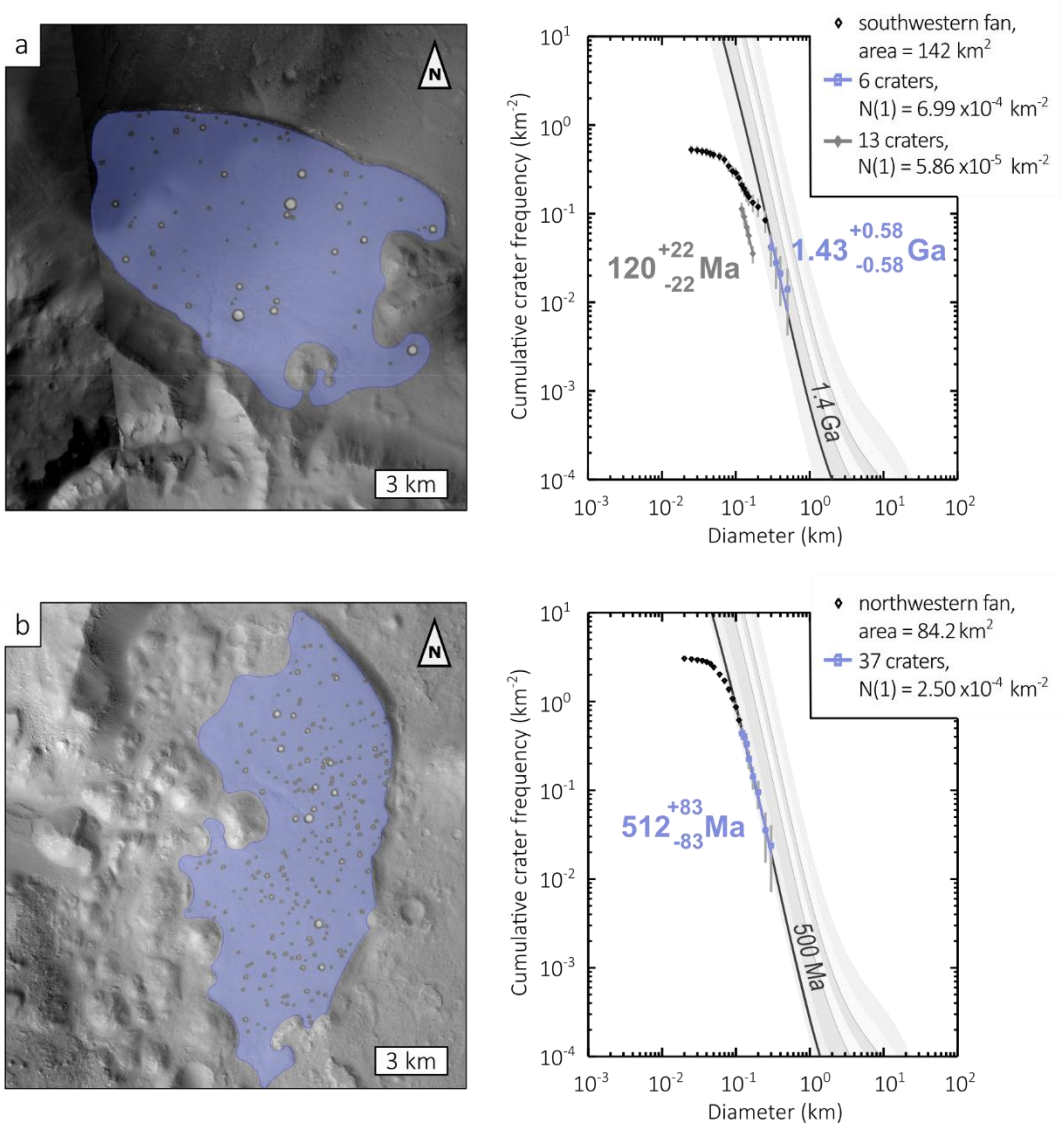

879

880 Figure 8 (1)

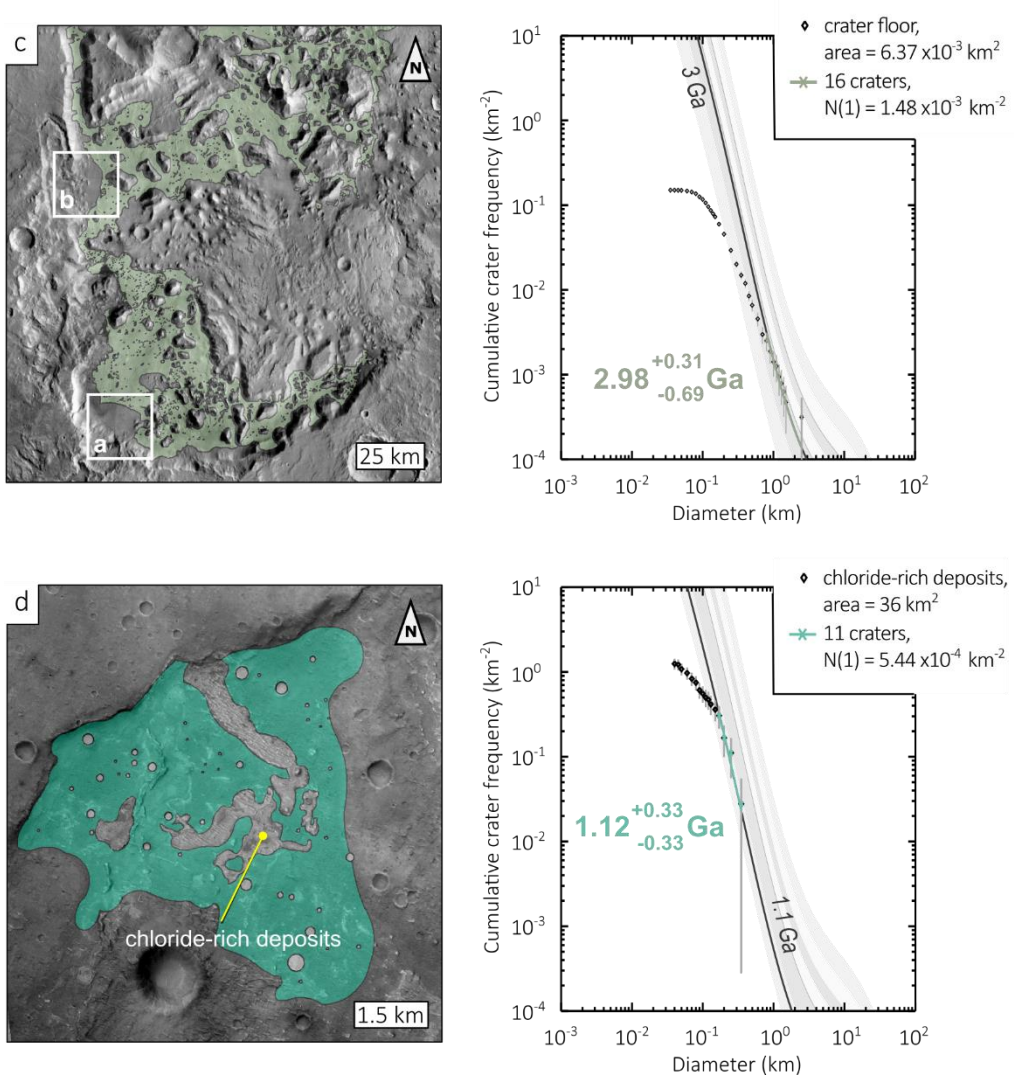

881
882 Figure 8 (2)

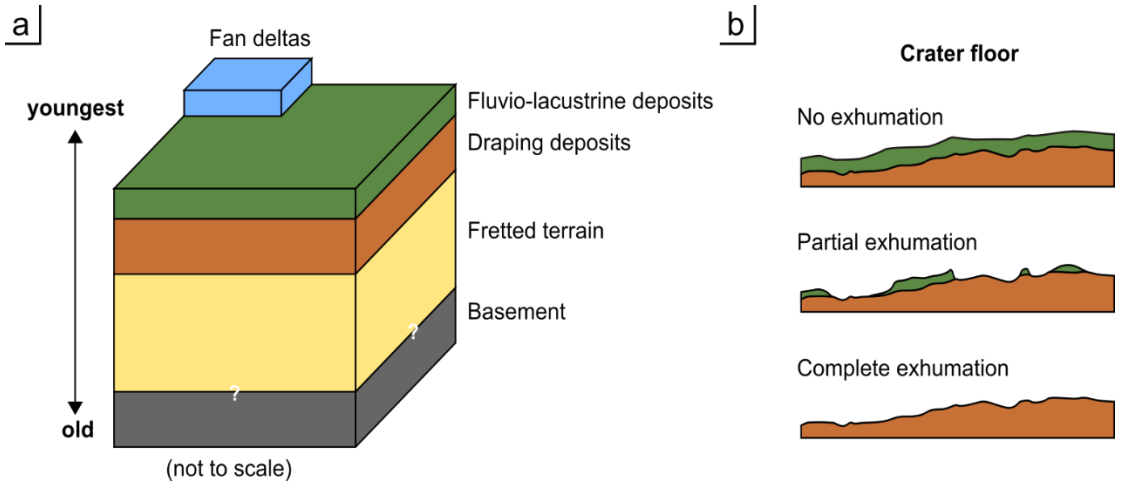

883

884 Figure 9

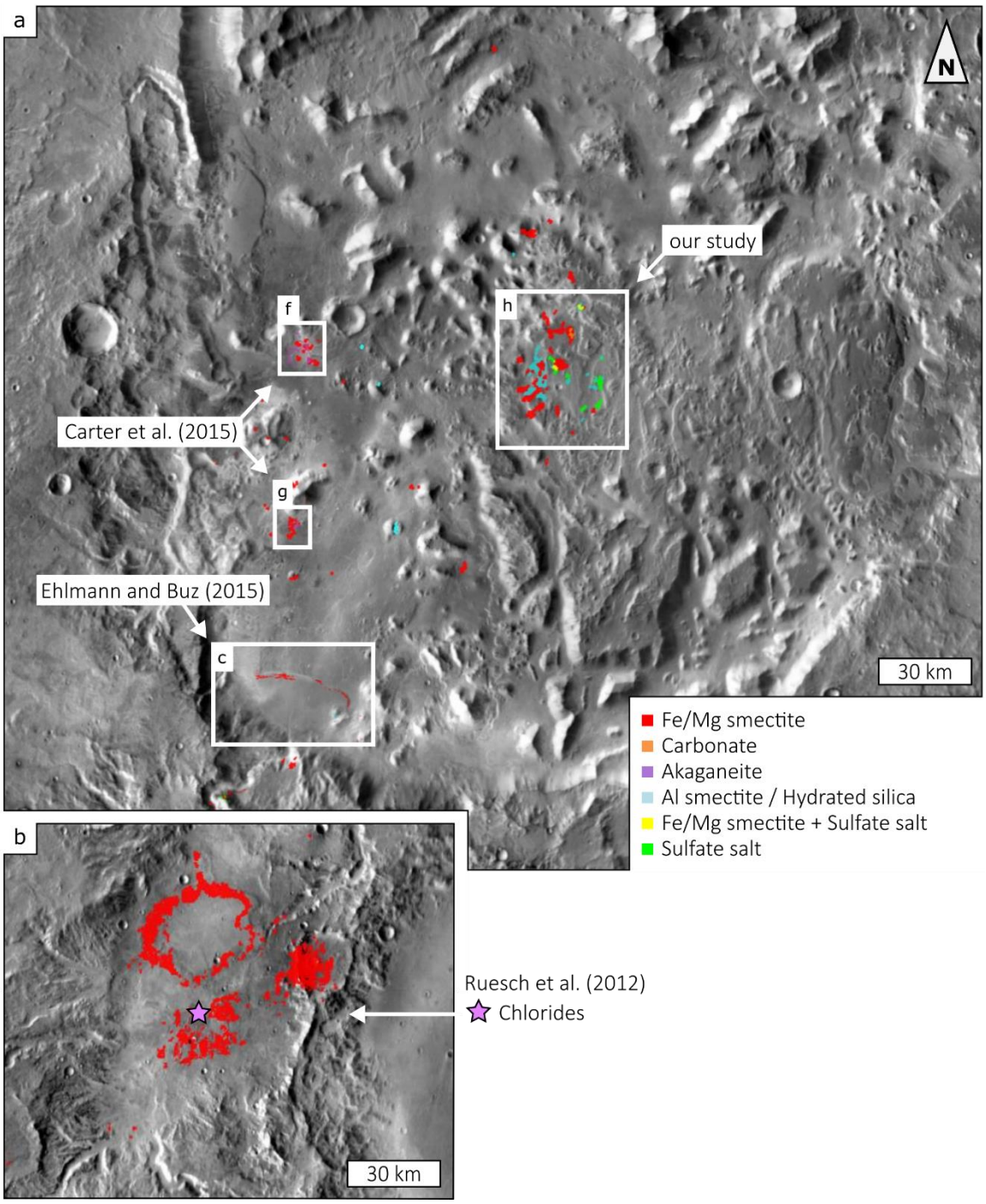

885

886 Figure 10 (1)

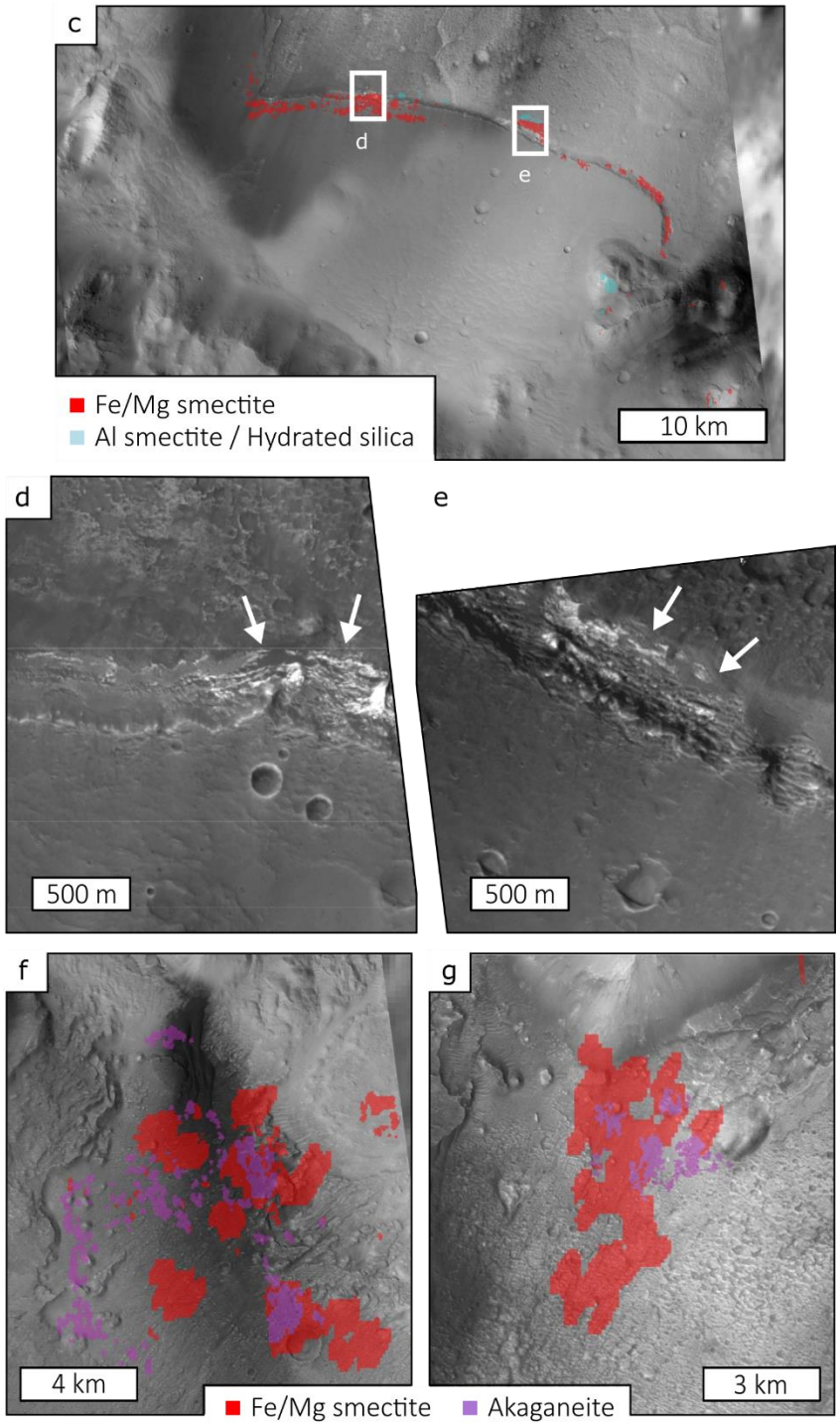

887

888 Figure 10 (2)

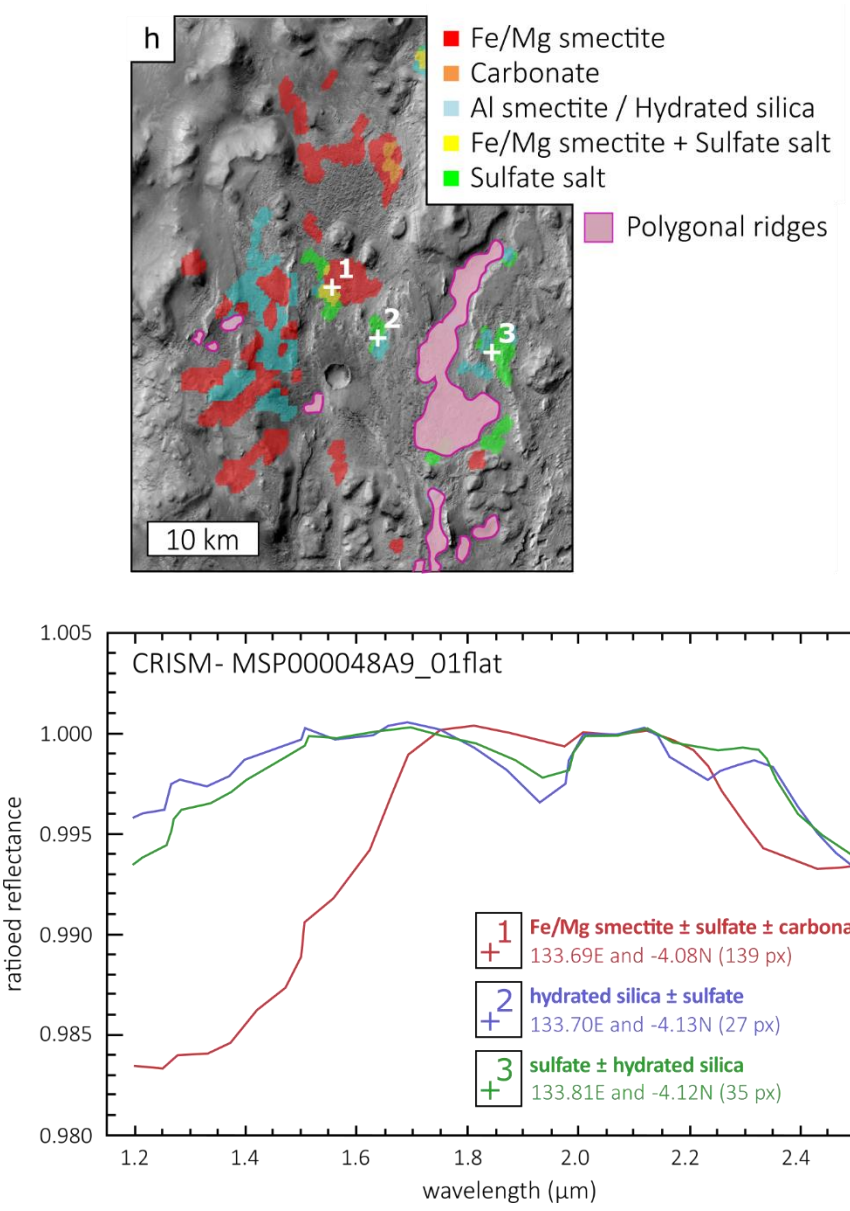
h
Fe/Mg smectite
Carbonate
Al smectite / Hydrated silica
Fe/Mg smectite + Sulfate salt
Sulfate salt
Polygonal ridges
1
2
3
10 km
CRISM- MSP000048A9_01flat
ratioed reflectance
wavelength (µm)
1.005
1.000
0.995
0.990
0.985
0.980
1.2
1.4
1.6
1.8
2.0
2.2
2.4
2.6
1 Fe/Mg smectite ± sulfate ± carbonates
133.69E and -4.08N (139 px)
2 hydrated silica ± sulfate
133.70E and -4.13N (27 px)
3 sulfate ± hydrated silica
133.81E and -4.12N (35 px)

Figure 10 (3)

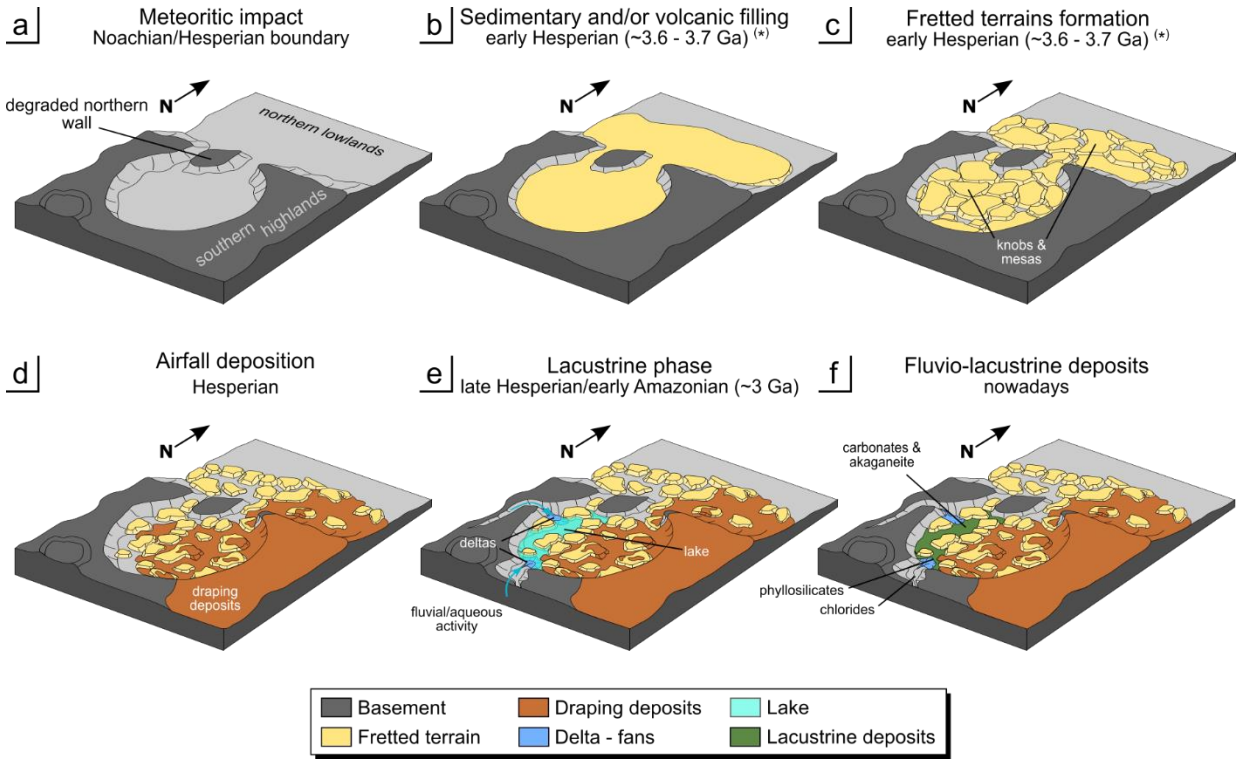

891

892 Figure 11